

# Dynamics after quenches in one-dimensional quantum Ising-like systems

Davide Rossini and Ettore Vicari

*Dipartimento di Fisica dell'Università di Pisa and INFN, Largo Pontecorvo 3, I-56127 Pisa, Italy*

(Dated: April 9, 2024)

We study the out-of-equilibrium dynamics of one-dimensional quantum Ising-like systems, arising from sudden quenches of the Hamiltonian parameter  $g$  driving quantum transitions between disordered and ordered phases. In particular, we consider quenches to values of  $g$  around the critical value  $g_c$ , and mainly address the question whether, and how, the quantum transition leaves traces in the evolution of the transverse and longitudinal magnetizations during such a deep out-of-equilibrium dynamics. We shed light on the emergence of singularities in the thermodynamic infinite-size limit, likely related to the integrability of the model. Finite systems in periodic and open boundary conditions develop peculiar power-law finite-size scaling laws related to revival phenomena, but apparently unrelated to the quantum transition, because their main features are generally observed in quenches to generic values of  $g$ . We also investigate the effects of dissipative interactions with an environment, modeled by a Lindblad equation with local decay and pumping dissipation operators within the quadratic fermionic model obtainable by a Jordan-Wigner mapping. Dissipation tends to suppress the main features of the unitary dynamics of closed systems. We finally address the effects of integrability breaking, due to further lattice interactions, such as in anisotropic next-to-nearest neighbor Ising (ANNNI) models. We show that some qualitative features of the post-quench dynamics persist, in particular the different behaviors when quenching to quantum ferromagnetic and paramagnetic phases, and the revival phenomena due to the finite size of the system.

## I. INTRODUCTION

The quantum evolution of many-body systems has been considered a challenging problem for long time. The recent experimental progress in the realization, control, and readout of the coherent dynamics of isolated quantum many-body systems (see e.g. Refs. [1, 2]) has made this issue particularly relevant for experiments and realizations of physical devices for quantum computing.

The simplest protocols in which the out-of-equilibrium dynamics of many-body systems can be investigated are provided by the so-called *quantum quenches* [3–8]. A quench protocol is generally performed within Hamiltonians that may be written as the sum of two noncommuting terms:  $\hat{H}(g) = \hat{H}_u + g\hat{H}_g$ , with a tunable parameter  $g$ . In practice, one may start from the ground state  $|\Phi_{g_0}\rangle$  of the Hamiltonian  $\hat{H}(g_0)$  associated with an initial value of the parameter  $g_0$ , i.e.  $|\Psi(t=0)\rangle = |\Phi_{g_0}\rangle$ , and then suddenly change it to  $g \neq g_0$ . Then the quantum evolution gets driven by the Hamiltonian  $\hat{H}(g)$ , that is,

$$|\Psi(t)\rangle = e^{-i\hat{H}(g)t}|\Phi_{g_0}\rangle \quad (1)$$

(hereafter we adopt units of  $\hbar = 1$ ). Several interesting issues have been investigated for the quantum dynamics after a quench. They include the long-time relaxation and the consequent spreading of quantum correlations and entanglement, the statistics of the work, localization effects due to the mutual interplay of interactions and disorder, dynamical phase transitions, the dynamic scaling close to quantum transitions, effects of dissipation due to interactions with an environment, the relevance of quantum measurements protocols after quenches at quantum transitions, to mention some of the most representative ones (see, e.g., Refs. [9–38] and references therein).

Quantum phase transitions are striking signatures of many-body collective behaviors [39, 40]. They are essentially related to the equilibrium low-energy properties of the system. However, they could also be probed by out-of-equilibrium dynamic protocols, for example analyzing the effects of slow changes of the Hamiltonian parameters across them [41–46]. Recently, some studies have also focused on the possibility of probing quantum transitions analyzing the out-of-equilibrium dynamics arising from quantum quenches, for example when instantaneously changing the Hamiltonian parameters, setting them to values corresponding to different quantum phases (see, in particular, Refs. [47–51]).

The out-of-equilibrium dynamics at the quantum transitions develops scaling behaviors controlled by the universality class of the quantum transition, located at a given  $g = g_c$ . Indeed such dynamic scaling is observed when the Hamiltonian parameters are slowly changed across the transition [16, 45, 46], and also at quantum quenches when both Hamiltonian parameters associated with the quench,  $g_0$  and  $g$ , are close to the quantum critical point [34, 52]. However, in the case of hard quenches, i.e. when  $g_0$  and  $g$  differ significantly, a dynamic scaling controlled by the universality class of the equilibrium quantum transition is not expected, essentially because the instantaneous change of the Hamiltonian parameters entails a significant amount of energy exchange. Indeed, the instantaneous change from  $g_0$  to  $g$  gives rise to a relatively large amount  $\Delta E$  of energy above the ground level of the Hamiltonian  $\hat{H}(g)$ ,

$$\Delta E = \sum_n [E_n(g) - E_0(g)] |\langle n, g | \Phi_{g_0} \rangle|^2 \sim L^d, \quad (2)$$

where  $L$  is the size of the system,  $|n, g\rangle$  and  $E_n(g)$  are the eigenstates and eigenvalues of  $\hat{H}(g)$ . Typically  $\Delta E$  is

much larger than the energy scale  $E_c$  of the low-energy excitations at criticality  $g = g_c$ , which is  $E_c \sim L^{-z}$  with  $z = 1$  for continuous transitions of Ising-like systems. This would naturally lead to the expectation that the unitary energy-conserving dynamics after quenching to  $g_c$  is not significantly related to the quantum critical features of the low-energy spectrum of the critical Hamiltonian. However, as argued in Refs. [47–51], some signatures may emerge as well. In particular, integrable many body systems (such as systems that are mappable into generic noninteracting fermionic systems) develop some peculiar discontinuities even in the asymptotic stationary states arising from the quantum quenches [47, 48]. On the other hand, local observables are not expected to present singularities in nonintegrable systems where generic quantum quenches lead to thermalization, since they are generally smooth functions of the temperature. Nonetheless it has been recently argued that it is possible to recover some signals from intermediate regimes of the quantum evolution after quenches [51].

In this paper we elaborate on this issue, focusing on the out-of-equilibrium dynamics arising from quantum quenches within one-dimensional Ising-like quantum systems. Specifically, we consider quantum XY chains, for which we observe peculiar nonanalyticities in the behavior of the transverse and longitudinal magnetizations, when comparing them after quenches of the Hamiltonian parameter  $g$  around the critical point. We also extend the analysis to finite-size effects, showing the emergence of revival phenomena with peculiar scaling behaviors. This somehow extends the phenomenology of quantum revival phenomena observed in various contexts, see e.g. Refs. [53–57]. Moreover, we discuss the impact of dissipative mechanisms arising from interactions with an environment, and the effects of integrability-breaking perturbations (such as next-to-nearest neighbor Ising-like couplings). Our purpose is to understand whether, and in which conditions, it is still possible to unveil signatures of the various equilibrium phases and quantum transitions separating them, after a quench protocol.

The paper is organized as follows. In Sec. II we present the XY chain, the dissipation modeling based on the Lindblad master equations, and the observables that we consider during the post-quench time evolution. Sec. III is devoted to the study of the dynamics arising from quenches starting from the disordered phase, in the thermodynamic limit and for finite-size systems with periodic and open boundary conditions. In Sec. IV we study the effects of dissipation due to the interaction with an environment within the quadratic fermionic model obtained by a Jordan-Wigner mapping of the Ising chain. In Sec. V we discuss quenches from the ordered states breaking the  $\mathbb{Z}_2$  symmetry of Ising-like systems. In Sec. VI we address some effects of integrability breaking, due to further lattice interactions, such as models with next-to-nearest neighbor couplings. Finally, in Sec. VII we summarize and draw our conclusions.

## II. THE XY MODEL AND OBSERVABLES

The ferromagnetic quantum XY chain is defined by the Hamiltonian

$$\hat{H}_{\text{XY}} = -\frac{J}{2} \sum_{x=1}^L \left[ (1+\gamma) \hat{\sigma}_x^{(1)} \hat{\sigma}_{x+1}^{(1)} + (1-\gamma) \hat{\sigma}_x^{(2)} \hat{\sigma}_{x+1}^{(2)} + g \hat{\sigma}_x^{(3)} \right], \quad (3)$$

where  $L$  is the number of lattice sites,  $\hat{\sigma}_x^{(\alpha)}$  denote the spin-1/2 Pauli matrices ( $\alpha = 1, 2, 3$ ) for each lattice site ( $x = 1, \dots, L$ ),  $J > 0$  is the energy scale,  $\gamma$  the Ising-like coupling anisotropy, and  $g$  the strength of a uniform transverse magnetic field. In the following we focus on positive values of  $g$ . For any  $\gamma > 0$ , a continuous quantum transition [40] belonging to the two-dimensional Ising universality class occurs at the critical point  $g = g_c = 1$ , separating a disordered ( $g > g_c$ ) from an ordered ( $g < g_c$ ) quantum phase. For  $\gamma = 1$ , one recovers the quantum Ising-chain Hamiltonian

$$\hat{H}_{\text{Is}} = -J \sum_{x=1}^L \left[ \hat{\sigma}_x^{(1)} \hat{\sigma}_{x+1}^{(1)} + g \hat{\sigma}_x^{(3)} \right]. \quad (4)$$

In the following we consider systems with boundary conditions respecting the  $\mathbb{Z}_2$  global symmetry of the model

$$\hat{\sigma}_x^{(1,2)} \rightarrow -\hat{\sigma}_x^{(1,2)}, \quad \hat{\sigma}_x^{(3)} \rightarrow \hat{\sigma}_x^{(3)}, \quad (5)$$

such as periodic boundary conditions (PBC), in which  $\hat{\sigma}_{L+x}^{(k)} = \hat{\sigma}_x^{(k)}$ , and open boundary conditions (OBC). Hereafter we set  $J = 1$ .

We want to study the dynamics arising from instantaneous quenches of the Hamiltonian parameter  $g$ , starting from states  $|\Psi(0)\rangle$  corresponding to the ground states associated with Hamiltonian parameters  $g_0 \neq g$ . In particular, as reference states, we consider the extreme cases of maximally disordered initial state  $|\rightarrow, \dots, \rightarrow\rangle$ , corresponding to the ground state for  $g_0 \rightarrow +\infty$  (i.e., all spins aligned along the direction  $\alpha = 3$ ), and the completely ordered state  $|\uparrow, \dots, \uparrow\rangle$ , corresponding to one of the degenerate lowest-energy states at  $g_0 = 0$  in the thermodynamic limit [i.e., all spins aligned along the direction  $\alpha = 1$  for the Ising model (4)]. Note that, in the latter case, the initial state breaks the  $\mathbb{Z}_2$  symmetry of the model.

For closed systems, the dynamics after a quench is unitary and the state at any time remains pure, as given by Eq. (1). In such case, to monitor the resulting out-of-equilibrium time evolution, we consider the longitudinal and transverse local magnetizations

$$M_x(t) = \langle \Psi(t) | \hat{\sigma}_x^{(1)} | \Psi(t) \rangle, \quad (6a)$$

$$S_x(t) = \langle \Psi(t) | \hat{\sigma}_x^{(3)} | \Psi(t) \rangle. \quad (6b)$$

In the case of boundary conditions and protocols respecting translational invariance, such as PBC or antiperiodic boundary conditions (ABC), the above magnetizations do not depend on the lattice site, thus

$$M(t) \equiv M_x(t), \quad S(t) \equiv S_x(t). \quad (7)$$

In the case of OBC, giving rise to inhomogeneous dependences, we distinguish the magnetizations at the center (c) of the chain and at the boundary (b), i.e,

$$M_c(t) \equiv M_{L/2}(t), \quad S_c(t) \equiv S_{L/2}(t), \quad (8a)$$

$$M_b(t) \equiv M_1(t), \quad S_b(t) \equiv S_1(t), \quad (8b)$$

where  $L$  has been assumed even, for the sake of clarity.

It is worth pointing out that the time dependence of the transverse magnetization is related to the average work  $W$  necessary to perform the following protocol: (i) the system is initially prepared in the ground state associated with a Hamiltonian transverse parameter  $g_0$ ; (ii) at  $t = 0$  one performs an instantaneous quench of the transverse parameter to  $g \neq g_0$ ; (iii) then the time evolution is driven by the Hamiltonian  $\hat{H}(g)$ ; (iv) after a time  $t_f$ , the transverse parameter is instantaneously brought back to  $g_0$ , and the system evolution is again driven by the initial Hamiltonian  $\hat{H}(g_0)$ . The total average work can be obtained as

$$W = E_f - E_i, \quad (9)$$

$$E_f = \langle \Psi(t \geq t_f) | \hat{H}(g_0) | \Psi(t \geq t_f) \rangle,$$

$$E_i = \langle \Psi(t = 0) | \hat{H}(g_0) | \Psi(t = 0) \rangle,$$

where we used the fact that, after  $t_f$ , the average energy is conserved along the unitary evolution. Straightforward calculations lead to the expression

$$W = (g - g_0) \sum_{x=1}^L [S_x(t_f) - S_x(0)]. \quad (10)$$

Thus, for translationally invariant systems, we obtain

$$W/L = (g - g_0) [S(t_f) - S(0)]. \quad (11)$$

If the system is in contact with some environment, the unitary evolution (1) is not valid anymore, because the time dependence is also determined by nonunitary drivings arising from the interaction with the environment. The state of the system at a given time  $t$  is represented by a density matrix  $\rho(t)$  whose time dependence can be reasonably described by the Lindblad master equation [58]

$$\frac{\partial \rho}{\partial t} = -i[\hat{H}(g), \rho] + u \mathbb{D}[\rho]. \quad (12)$$

The first term in the right-hand side provides the coherent driving, while the second term accounts for the coupling to the environment, characterized by a global coupling constant  $u > 0$ . In our quench protocol, the initial state can be thus written as  $\rho(t = 0) = |\Phi_{g_0}\rangle\langle\Phi_{g_0}|$ . The instantaneous longitudinal and transverse magnetizations now read

$$M_x(t) = \text{Tr}[\hat{\sigma}_x^{(1)} \rho(t)], \quad S_x(t) = \text{Tr}[\hat{\sigma}_x^{(3)} \rho(t)]. \quad (13)$$

Analogous definitions as those in Eqs. (7), (8a), (8b), can be adopted here as well, depending on the choice of the boundary conditions.

### III. QUENCHES STARTING FROM THE DISORDERED PHASE

We first focus on the unitary dynamic behavior of closed systems which arises from instantaneous changes of the transverse parameter  $g$ , starting from the ground state associated with an initial value  $g_0 > 1$  in the disordered phase. By symmetry, the longitudinal magnetization remains zero at any time after the quench,  $M_x(t) = 0$ , while the transverse magnetization  $S_x(t)$  presents a nontrivial time dependence [9, 10]. We initially discuss the case of PBC for which  $S(t) \equiv S_x(t)$  independently of the lattice site, and then that of OBC, for which we present results for both the central and boundary local transverse magnetizations,  $S_c$  and  $S_b$  respectively.

A representative example is shown in Fig. 1, for an instantaneous quench to  $g_c$ , starting from the fully polarized state along the transverse direction, which corresponds to the ground state  $|\Phi_{g_0 \rightarrow \infty}\rangle$ . The considered system is subject to PBC. The time evolutions of the transverse magnetization for the sizes  $L = 500$  and  $L = 1000$  appear identical up to  $t \lesssim 100$ . Within this interval the curves rapidly converge toward the value  $S(\infty) = 0.5$  (see inset of Fig. 1), in a time interval  $t \lesssim 10$ , and then appear constant up to  $t \approx 100$ . Since data for  $L = 500$  and  $L = 1000$  match, this behavior should correspond to the time dependence in the thermodynamic limit  $L \rightarrow \infty$ . However, after such a relatively large interval, where the systems have apparently reached their stationary behavior,

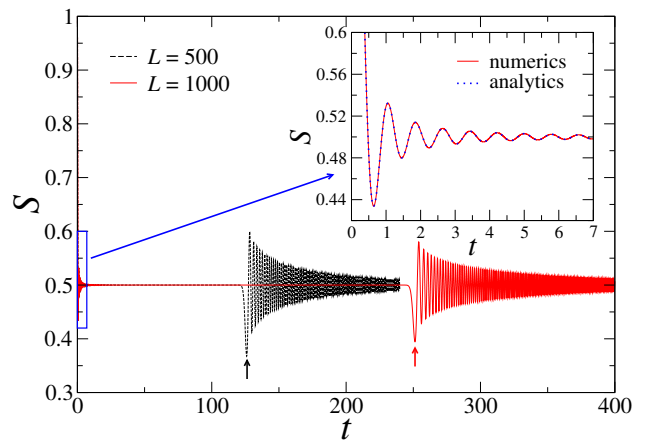


FIG. 1: Transverse magnetization  $S(t)$  after a quench in the quantum Ising chain with PBC, starting from a completely disordered state ( $g_0 = +\infty$ ), to  $g = 1$  (critical point), for  $L = 500$  up to  $t = 240$  (dashed black line), and for  $L = 1000$  up to  $t = 400$  (continuous red line). At relatively small times,  $t < 100$ , the data sets superimpose, corresponding to the thermodynamic limit, while after some time which depends on the size, in particular after  $t \approx L/(2v_m)$  with  $v_m = 2 \min[g, 1] = 2$  (indicated by the arrows), peculiar oscillating behaviors appear, corresponding to finite-size revivals. The inset shows a magnification at small times (blue box), where numerical data have been superimposed with the analytic results in the thermodynamic limit (dotted blue line) obtained in Ref. [10].

ior, the time dependence becomes again nontrivial. It shows peculiar structures at later times depending on the size, starting from  $t \approx 125$  for  $L = 500$  and  $t \approx 250$  for  $L = 1000$ , thus at larger and larger times with increasing the size. These are characterized by an oscillatory behavior enveloped by a smooth decreasing function, and are clearly finite-size effects. In the following we characterize the two regimes, identifying their main features. We conclude this brief summary by noticing that Fig. 1 reports the results for a chain with PBC, but analogous qualitative considerations apply to different boundary conditions as well (see, e.g., Sec. III C for the case with OBC).

### A. Time dependence in the thermodynamic limit

The time dependence of the transverse magnetization in the thermodynamic limit was analytically computed long time ago by Niemeijer [9] and by Barouch, McCoy, and Dresden [10]. The infinite-size limit of the transverse magnetization,

$$\Sigma(t, g_0, g) \equiv S(t, g_0, g, L \rightarrow \infty), \quad (14)$$

can be written as a sum of an asymptotic time-independent term and a time dependent term vanishing in the large-time limit, i.e.

$$\Sigma(t, g_0, g) = F(g_0, g) + F_t(t, g_0, g). \quad (15)$$

Setting

$$\Lambda(k, g) = \sqrt{[g - \cos(k)]^2 + \gamma^2 \sin(k)^2}, \quad (16)$$

Ref. [10] reports

$$F(g_0, g) = \int_0^\pi \frac{dk}{\pi} \frac{g - \cos(k)}{\Lambda(k, g_0) \Lambda(k, g)^2} \times \{ [g_0 - \cos(k)][g - \cos(k)] + \gamma^2 \sin(k)^2 \}, \quad (17a)$$

and

$$F_t(t, g_0, g) = \int_0^\pi \frac{dk}{\pi} \frac{\gamma^2 (g_0 - g) \sin(k)^2 \cos[4\Lambda(k, g)t]}{\Lambda(k, g_0) \Lambda(k, g)^2}. \quad (17b)$$

In particular, for  $g_0 \rightarrow \infty$  these expressions simplify into

$$F(\infty, g) = \int_0^\pi \frac{dk}{\pi} \frac{[g - \cos(k)]^2}{\Lambda(k, g)^2}, \quad (18a)$$

$$F_t(t, \infty, g) = \int_0^\pi \frac{dk}{\pi} \frac{\gamma^2 \sin(k)^2 \cos[4\Lambda(k, g)t]}{\Lambda(k, g)^2}. \quad (18b)$$

Let us first focus on the large-time limit (17a) of  $\Sigma(t)$ . As shown by the plots in Fig. 2, the function  $F(g_0, g)$  presents a nonanalytic behavior in correspondence of the critical point  $g_c = 1$ . Indeed, we have that

$$\lim_{g \rightarrow g_c^+} \frac{\partial F(g_0, g)}{\partial g} - \lim_{g \rightarrow g_c^-} \frac{\partial F(g_0, g)}{\partial g} = \gamma^{-1/2}. \quad (19)$$

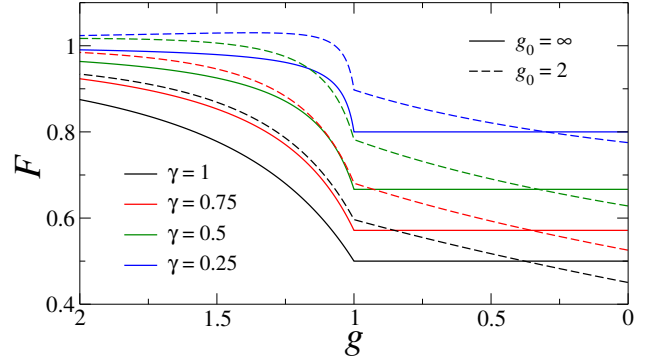


FIG. 2: The function  $F(g_0, g)$  of Eq. (17a) representing the large-time limit of the transverse magnetization in the thermodynamic limit [10], as a function of  $g$ , for various values of  $\gamma$  (different colors, see legend), and  $g_0 = \infty$  (continuous lines) or  $g_0 = 2$  (dashed lines). The curves display a singular behavior, i.e. a discontinuity in the derivative, at  $g = g_c = 1$ .

Note that such a discontinuity is independent of  $g_0 > 1$ . In particular, for  $\gamma = 1$  and  $g_0 \rightarrow \infty$ , the behavior around  $g_c$  turns out to be

$$F(\infty, g) = \begin{cases} \frac{1}{2} + (g-1) + O[(g-1)^2] & \text{for } g > 1, \\ \frac{1}{2} & \text{for } g \leq 1. \end{cases} \quad (20)$$

An analogous discontinuity has been reported in Ref. [47] for the asymptotic behavior of the energy density after a quench, and also in generic noninteracting fermionic systems [48].

Even the asymptotic approach to the large-time limit is singular at  $g_c$ . Indeed for  $g \neq 1$  it is given by [10, 21]

$$F_t(t, g_0, g) = \frac{g_0 - g}{2^{7/2} \sqrt{\pi} g^{3/2}} t^{-3/2} \times \left[ \frac{\sin[4(g+1)t - \pi/4]}{(g_0 + 1)\sqrt{g+1}} - \frac{\sin[4|g-1|t + \pi/4]}{|g_0 - 1|\sqrt{|g-1|}} \right] + O(t^{-5/2}), \quad (21)$$

while at  $g = 1$  it turns out to be given by

$$F_t(t, g_0, 1) = \frac{(g_0 - 1) \sin(8t - \pi/4)}{16(g_0 + 1)\sqrt{\pi}} t^{-3/2} + O(t^{-5/2}). \quad (22)$$

Note that Eq. (22) is simply obtained by dropping the second divergent term within the parenthesis in Eq. (21). Numerical evidence of the validity of Eq. (22), for sufficiently long times, is provided by the data shown in Fig. 3. There we report a direct comparison between the transverse magnetization  $\Sigma(t, g_0, g)$  of Eq. (15), calculated either with the exact formula of Eq. (17b) or with the approximate one of Eq. (22). The agreement between the two results emerges from the analysis of the absolute discrepancy between them, explicitly shown in the inset, where corrections of  $O(t^{-5/2})$  evidently appear (see dot-dashed blue line).

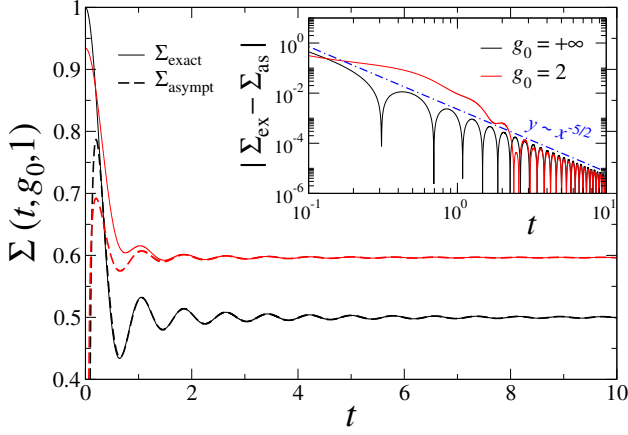


FIG. 3: Time behavior of the transverse magnetization  $\Sigma(t, g_0, g)$  in the infinite-size limit, for a quench in the quantum Ising chain from two different values of  $g_0$  (see legend), to the critical point  $g = 1$ . Continuous lines denote the exact result obtained using Eq. (17b), while dashed lines report the approximate result using Eq. (22). The inset shows absolute discrepancies between exact and approximate results; the dot-dashed blue line denotes a  $t^{-5/2}$  behavior and is plotted to guide the eye.

We finally recall that the thermodynamic limit, approached by taking the large- $L$  limit at fixed time, is expected to be independent of the boundary conditions. This is confirmed by our numerical results. However, as we shall see below, the finite-size effects are instead dependent on the boundary conditions. In the following we address the cases of PBC and OBC separately.

### B. Finite-size effects with PBC

We now discuss the emergence of finite-size effects mostly related to revival phenomena, which are characterized by definite power-law scaling behaviors. Analyses of revival finite-size effects have been recently discussed under various perspectives in Refs. [17, 18, 22, 57], considering also the behavior of the entanglement properties. Here we focus on the quantum Ising chain (4) with PBC.

Before presenting our results, it is instructive to realize that, for quenches starting from ground states for  $g_0 > g_c$ , the dynamic problem can be exactly mapped into that of a fermionic quadratic model with antiperiodic boundary conditions (ABC), see e.g. Ref. [59]. This is essentially due to the fact that the initial quantum state  $|\Phi_{g_0 > g_c}\rangle$  has a definite parity, and therefore only fermionic states with ABC are involved during the evolution. Therefore, for these types of quenches, we may consider the equivalent Kitaev quantum wire defined by the Hamiltonian [60]

$$\hat{H}_K = - \sum_{x=1}^L (\hat{c}_x^\dagger \hat{c}_{x+1} + \gamma \hat{c}_x^\dagger \hat{c}_{x+1}^\dagger + \text{h.c.}) - 2g \sum_{x=1}^L \hat{n}_x, \quad (23)$$

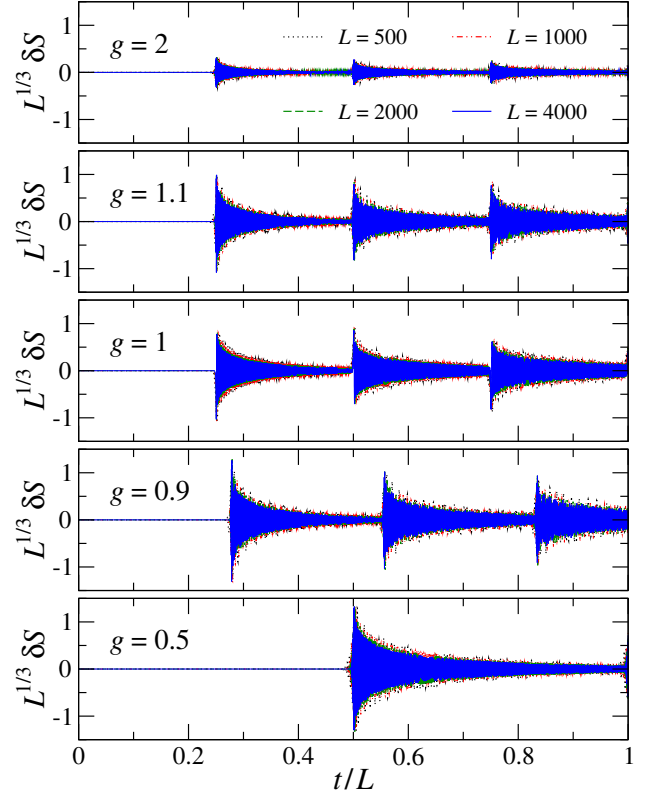


FIG. 4: Finite-size features of the temporal behavior of the transverse magnetization after a quench from  $g_0 = +\infty$ . We plot  $L^{1/3} \delta S$  versus the rescaled time  $t_L \equiv t/L$ , where  $\delta S$  is defined in Eq. (24). Different panels are for  $g = 2, 1.1, 1, 0.9, 0.5$ . Colored curves stand for various system sizes, as indicated in the legend, and nicely support the behavior put forward in Eq. (25).

where  $\hat{c}_x$  is the fermionic annihilation operator on the  $x$ th site of the chain and  $\hat{n}_x \equiv \hat{c}_x^\dagger \hat{c}_x$  the density operator. The quench problem considered here can be matched by taking ABC,  $\hat{c}_{L+x} = -\hat{c}_x$  (we suppose  $L$  even, for convenience). The straightforward diagonalization of the quadratic fermionic model (23) allows one to obtain results for very large sizes, up to  $L = O(10^4)$ , requiring computational resources which increase only linearly with  $L$ . For details see, e.g., Refs. [46, 59]. In the following we set  $\gamma = 1$ , corresponding to the Ising chain (4).

Some results for quenches from  $g_0 \rightarrow \infty$  to various values of  $g$  are shown in Fig. 4, where we report the subtracted transverse magnetization

$$\delta S(t, g_0, g, L) \equiv S(t, g_0, g, L) - \Sigma(t, g_0, g), \quad (24)$$

$\Sigma(t, g_0, g)$  being the infinite-size limit given by Eq. (14). The numerical results show the following behavior

$$\delta S(t, L) = L^{-a} f_e(t_L) f_o(t, L) + O(L^{-1}), \quad (25)$$

where

$$t_L \equiv t/L, \quad a = 1/3 \quad (26)$$

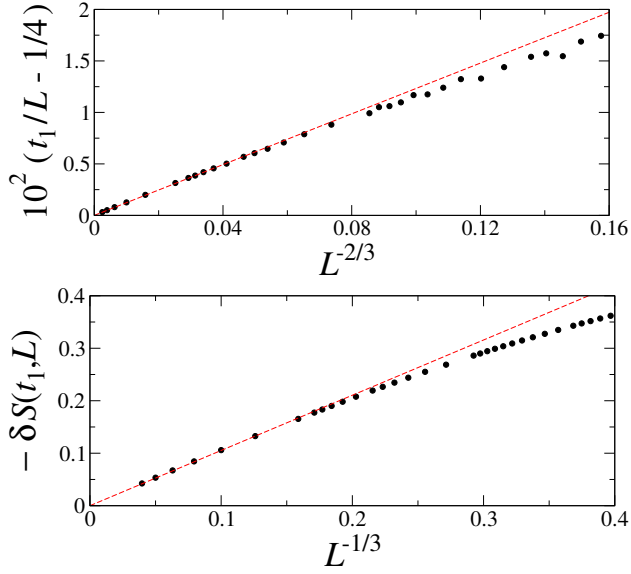


FIG. 5: Scaling behavior of the position and height of the first dip (located at  $t_1 \approx L/4$ , corresponding to  $t_{L,1} \equiv t_1/L \approx 1/4$ ) of the transverse magnetization for quenches to the critical point  $g = 1$ , starting from the fully disordered state  $|\Phi_\infty\rangle$  (see arrows in Fig. 1). We simulated systems with up to  $L = 10^4$  sites. Upper panel: data for  $t_{L,1} - 1/4$  vs.  $L^{-2/3}$ , confirming the behavior predicted by Eq. (28); the dashed red line shows a linear fit for  $L \geq 100$ . Lower panel: data for  $\delta S(t_1, L)$  vs.  $L^{-1/3}$ ; the dashed red line shows a linear fit for  $L \geq 250$ .

(as we shall see, the accuracy of the estimate of exponent  $a$  is very high),  $f_o(t, L)$  is a rapidly oscillating function around zero depending on both  $t$  and  $L$ , while the envelope function  $f_e$  is a (non-oscillating) function of  $t_L$  with discontinuities located at  $t_L = t_{L,k}$  [for simplicity, here we have omitted the dependence on  $g_0$  and  $g$  in Eq. (25)].

The discontinuities of  $f_e$  are essentially related to revival phenomena and appear at times

$$t_{L,k} \equiv \frac{k}{2v_m}, \quad v_m = 2 \text{Min}[g, 1], \quad (27)$$

for  $k = 1, 2, \dots$ , where  $v_m$  is the maximum velocity of the quasi-particle modes [20, 61, 62]. The amplitude of such discontinuities generally tends to decrease with increasing  $k$ , as it can be seen from the various panels of Fig. 4. We point out that the scaling behavior of the revival times  $t_{L,k}$ , and their connection with the maximum velocity of the quasi-particle modes, were already put forward by other studies of revival phenomena in finite-size systems, see e.g. Refs. [18, 22, 57].

Our numerical results for  $g = g_c = 1$  show that the first sharp dip is asymptotically located at

$$t_{L,1} = 1/4 + O(L^{-2/3}), \quad (28)$$

as reported in the upper panel of Fig. 5. The relative accuracy achieved by our numerical results on the asymptotic location of the peak is very high, within  $O(10^{-5})$ , so that we can safely conclude that its value is  $1/4$  with

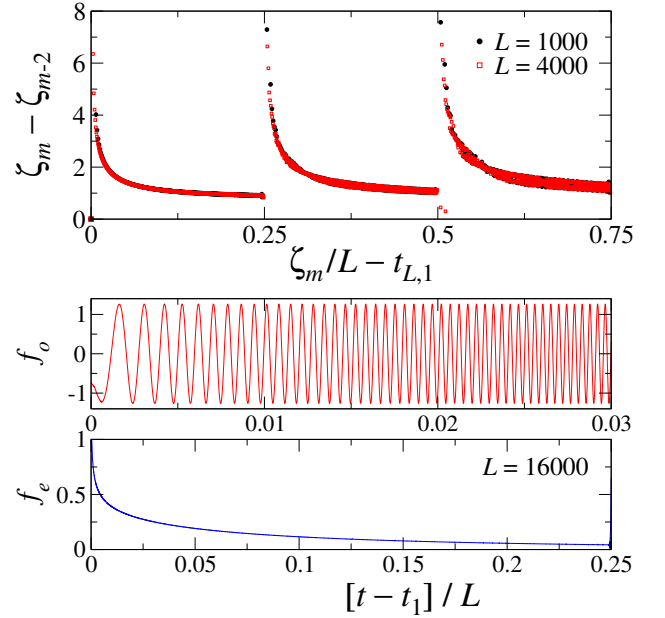


FIG. 6: Numerical analysis of the oscillations appearing in the time behavior of  $\delta S(t, L)$ , after a quench from the completely disordered state to  $g_c$ . Top panel: temporal interval  $\zeta_m - \zeta_{m-2}$  between the times at which the  $m$ th zero and the  $(m-2)$ th zero occur, for two different sizes  $L$ . This is plotted as a function of the rescaled time  $\zeta_m/L - t_{L,1}$ . Central panel: time behavior of the oscillating function  $f_o$ , numerically inferred by taking the ratio between  $L^{1/3}\delta S(t, L)$  at a given size  $L$  ( $L = 4000$  in the figure) and the interpolation of the maxima of the corresponding curve for the largest available data set at  $L = 16000$ . The latter also gives an estimate of the envelope function  $f_e$ , reported in the bottom panel.

great accuracy. This can be related to the interference between the signals traveling in the opposite direction with velocity  $v_m = 2$ , [54] taking a time  $t = L/(2v_m) = L/4$  to approach each other. Note that the  $O(L^{-2/3})$  corrections to the value of  $t_L$  at the dip arise from the  $O(L^{-1})$  corrections in the formula (25). We mention that, once fixed the asymptotic value  $t_{L,1} = 1/4$ , the relative accuracy of the estimate of the exponent of the power-law correction in Eq. (28) is a few per mille. The lower panel of Fig. 5 shows the large- $L$  scaling of the transverse magnetization at the dip, clearly demonstrating the power-law asymptotic behavior  $L^{-a}$  with  $a = 1/3$ , which is approached with  $O(L^{-2/3})$  corrections, as implied by Eq. (25). The relative accuracy on the estimate of  $a$  turns out to be safely better than  $10^{-4}$ . Therefore, somehow biased by the expectation that the exponent  $a$  should be a simple fraction, we assume  $a = 1/3$  in the following.

The zeroes of  $\delta S$ , cf. Eq. (25), are essentially controlled by the oscillating function  $f_o$ . In Fig. 6 we show some analyses of the results for quenches to  $g = g_c = 1$ . The top panel displays numerical results for the zeroes  $\zeta_m$  of the function  $\delta S$ . The difference  $\zeta_m - \zeta_{m-2}$ , which would correspond to the period in the case of periodic functions, turns out to be a function of  $t_L \equiv t/L$ , with singularities



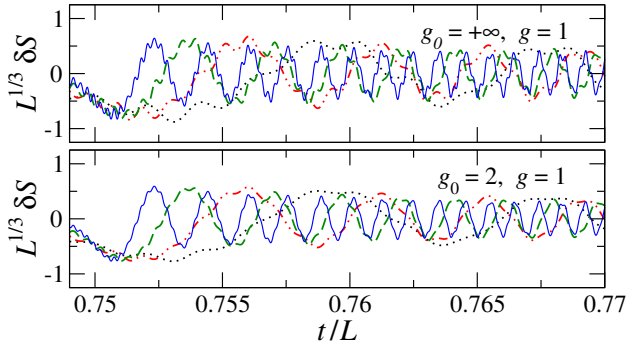


FIG. 7: Finite-size features of the temporal behavior of the transverse magnetization after a quench to the critical point  $g = 1$ , starting from either  $g_0 = +\infty$  (upper panel) or  $g_0 = 2$  (lower panel). We plot curves for  $\delta S(t, g_0, g, L)$  as defined in Eq. (24), zooming around the third revival [see Eq. (27)]. Note that the upper panel displays the same data of the central panel of Fig. 4. The color code is the same as in that figure.

at  $t_{L,k}$ . The bottom panel shows the envelop function  $f_e$  as obtained by interpolating the maxima of  $L^{1/3}\delta S$  for the largest available lattice size  $L = 16000$ , while the intermediate panel shows the resulting oscillatory function  $f_o$ . The above results globally support the ansatz (25).

We note that the scaling behavior (25) is generally observed for any value of  $g$ , as confirmed by our numerical simulations (not shown here). Of course, the functions  $f_e$  and  $f_o$  will depend on  $g$ , but their structure looks similar when varying it. Therefore, this shows that the main features of the finite-size effects are not related to the existence of quantum criticality at  $g_c$ . We also mention that analogous results, reproduced by Eq. (25) with the appropriate dependence on  $g_0$  and  $g$ , are obtained when starting from ground states corresponding to finite values of  $g_0 > 1$ . Indeed, comparing the two panels of Fig. 7, obtained for quenches starting from either  $g_0 = +\infty$  or  $g_0 = 2$ , one can recognize the same scaling behavior for the curves corresponding to various system sizes. Note that times have been zoomed around  $t/L \approx 0.75$ , in order to highlight the third revival phenomena appearing at time  $t_3$  [see Eq. (27)]. A close look at the two panels reveals that, although very similar patterns can be seen for the two cases, fast oscillating wiggles are slightly reduced for  $g_0 = 2$ . Such differences are even less visible for the former two revivals (not shown).

We finally mention that finite-size revivals in the entanglement entropy were investigated in Ref. [57], showing that they are also characterized by dips in the block entanglement entropy.

### C. Finite-size effects with OBC

A natural arising issue concerns the dependence on the boundary conditions of the main features observed in the previous sections. To answer this question, we have con-

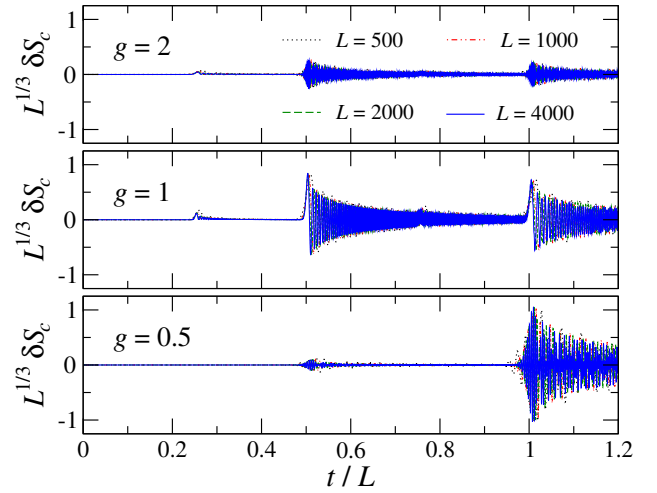


FIG. 8: Finite-size features of the temporal behavior of the central transverse magnetization, with OBC, after a quench from  $g_0 = +\infty$  to  $g = 2$  (upper),  $g = 1$  (central), and  $g = 0.5$  (lower panel). We show curves for  $L^{1/3}\delta S_c$  versus the rescaled time  $t_L \equiv t/L$ , where  $\delta S_c(t, L)$  is defined in Eq. (29).

sidered quench protocols applied to systems with OBC. Here we report results starting from the fully disordered state  $|\Phi_{+\infty}\rangle$ , focusing again on the transverse magnetization. However, since OBC breaks the translational invariance, we will separately consider the central and boundary local transverse magnetizations, cf. Eqs. (8a) and (8b), as representative observables. Technically, we can still take advantage of the mapping into the Kitaev quantum wire, where ABC are now replaced by OBC. However, in this latter case, going to Fourier space is no longer helpful to diagonalize the Hamiltonian  $\hat{H}_K$  and one has to perform a  $2L$ -dimensional Bogoliubov rotation. The required computational resources keep growing polynomially with  $L$ , thus preserving the ability to simulate sizes comparable to those for translationally invariant systems.

The central local transverse magnetization is expected to have the same large- $L$  limit discussed for systems with PBC. We have also checked it numerically. Thus, to study finite-size effects, we again subtract the asymptotic large- $L$  limit  $\Sigma$  given by Eq. (15), i.e.

$$\delta S_c(t, g_0, g, L) = S_c(t, g_0, g, L) - \Sigma(t, g_0, g), \quad (29)$$

with  $S_c$  defined as in Eq. (8a). The transverse magnetization  $S_b$  at the boundary, cf. Eq. (8b), is expected to behave differently, even in the large- $L$  limit, and its time dependence in the thermodynamic limit is not known.

Fig. 8 reports the central transverse magnetization at the central site of the chain, when the time evolution is controlled by the Hamiltonian at  $g = 2$ ,  $g = 1$ , and  $g = 0.5$ , starting from the disordered state  $|\Phi_{+\infty}\rangle$ . The finite-size behavior of  $S_c$  is qualitatively similar to that observed for systems with PBC. Indeed, the large- $L$  time dependence of the subtracted central transverse magne-

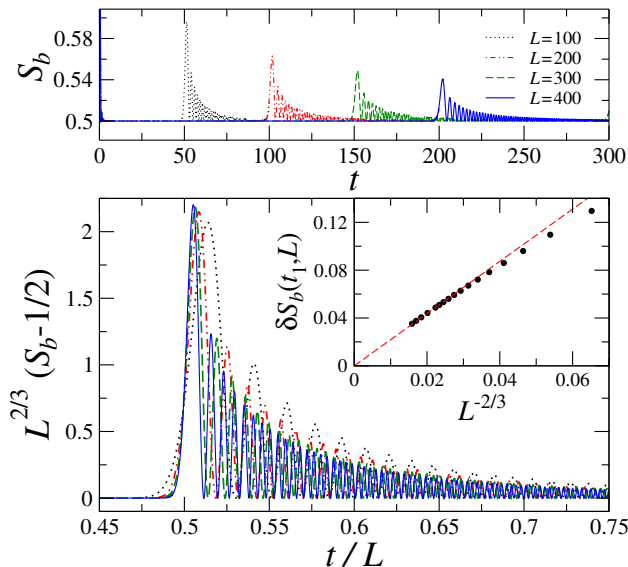


FIG. 9: Finite-size features of the temporal behavior of the boundary transverse magnetization, with OBC, after a quench from  $g_0 = +\infty$  to  $g = 1$ . The top panel shows curves for  $S_b$  versus the time  $t$ , while the bottom panel shows curves for  $L^{2/3}\delta S_b$  [cf. Eq. (31)] versus the rescaled time  $t_L \equiv t/L$ . The inset of the bottom panel highlights the scaling behavior of the height of the first peak (located at  $t_1 \approx L/2$ ), showing data for  $\delta S_b(t_1, L)$  vs.  $L^{-2/3}$ ; the dashed red line is a linear fit for  $L \geq 240$ .

tization  $\delta S_c$  turns out to be well described by

$$\delta S_c(t, L) = L^{-a} f_e(t_L) f_o(t, L) + O(L^{-1}) \quad (30)$$

with  $a = 1/3$ , analogously to the PBC case [cf. Eq. (25)]. We also note that, apart from rapid oscillations encoded by the function  $f_o(t, L)$ , smooth envelope structures appear, associated with a rescaled time  $t_L = t/L$ . Again peculiar discontinuities emerge in proximity of the values  $t_{L,k} = kL/(2v_m)$ , for  $k = 1, 2, \dots$ . The main difference with the PBC case is that at  $t_{L,1}$  only oscillations with tiny amplitudes emerge. More in general, the main structures are observed at times  $t_{L,2j}$  ( $j = 1, 2, \dots$ ); small bumps also occur at any time  $t_{L,2j-1}$ , although they are barely visible for  $j \geq 2$ .

The behavior of the boundary transverse magnetization is substantially different. Let us define again a subtracted quantity

$$\delta S_b(t, L) \equiv S_b(t, L) - S_b(t, L \rightarrow \infty) \quad (31)$$

where  $S_b(t, L \rightarrow \infty)$  can be accurately obtained from the results for the largest lattices, as one may infer from the curves shown in the upper panel of Fig. 9. In particular, we have verified that the apparent relation  $S_b = S_c$  for  $t \rightarrow \infty$  and  $L \rightarrow \infty$  actually holds only for  $g_0 \rightarrow \infty$ , and, even in this case, the equality does not hold at finite  $t$ . Finite-size effects are captured by a scaling equation of the form

$$\delta S_b(t, L) = L^{-b} f_e(t_L) f_o(t, L) + O(L^{-1}), \quad (32)$$

where

$$b \approx 2/3, \quad (33)$$

as emerging from the data reported in the lower panel. This behavior is again characterized by the rapid oscillations  $f_o(t, L)$  and a smooth envelope function  $f_e(t_L)$  with argument  $t_L = t/L$ . The main difference is that such a smooth finite-size behavior gets suppressed by a power  $L^{-2/3}$  (see, in particular, the inset in the lower panel), and peculiar structures emerge at  $t_{L,k} = k/v_m$ .

We conclude this part by mentioning that the above behaviors are not peculiar of the choice of the initial condition, corresponding to the ground state for  $g_0 \rightarrow \infty$ . Indeed, their main features also emerge in quenching protocols starting from ground states associated with finite values  $g_0 > 1$  (data not shown).

#### IV. QUENCHES FROM THE DISORDERED PHASE IN THE PRESENCE OF DISSIPATION

##### A. Modeling dissipation

The purpose of this section is to extend the previous analysis on the dynamic features of closed quantum Ising chains, in order to include the effects of weak dissipative mechanisms: besides the changes of the Hamiltonian parameters, we suppose that the many-body system is also subject to some interaction with the environment. For the sake of simplicity, here we only concentrate on quenches starting from the disordered phase ( $|g_0| > 1$ ), such that it is still possible to exploit the mapping to the Kitaev Hamiltonian for fermionic particles (23), as we did in Sec. III B and III C. We consider dissipation mechanisms associated with either particle losses or pumping on each lattice site, so that our system-bath coupling scheme describes the coupling of each site with an independent bath. In the case of weak coupling to Markovian baths, the general Lindblad master equation (12) can be thus written as [63, 64]

$$\frac{\partial \rho}{\partial t} = -i[\hat{H}_K, \rho] + u \sum_j \left[ \hat{L}_j \rho \hat{L}_j^\dagger - \frac{1}{2}(\rho \hat{L}_j^\dagger \hat{L}_j + \hat{L}_j^\dagger \hat{L}_j \rho) \right]. \quad (34)$$

The onsite Lindblad operators associated to either losses (l) or pumping (p) are respectively given by [36, 65–69]:

$$\hat{L}_j^{(l)} = \hat{c}_j, \quad \hat{L}_j^{(p)} = \hat{c}_j^\dagger. \quad (35)$$

The choice of such dissipators turns out to be particularly convenient for the numerical analysis, allowing us to maintain the polynomial scaling with  $L$  of the computational complexity of the problem, as for the unitary dynamics of the Kitaev chain.

In the rest of this section, for our convenience we shall restrict to homogeneous dissipation mechanisms and to Kitaev models with ABC (corresponding to PBC for the



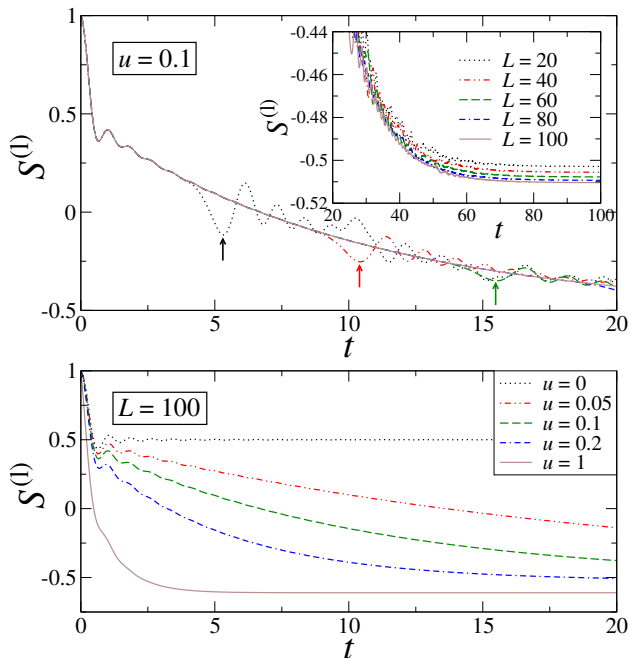


FIG. 10: Time behavior of the transverse magnetization  $S^{(l)}$  after a quench in the Kitaev quantum wire, starting from a completely filled state ( $g_0 = +\infty$ ), to  $g = g_c = 1$  (critical point), in the presence of incoherent particle losses. Upper panel: curves are for different sizes  $L$ , at fixed dissipative coupling constant  $u = 0.1$  (the inset shows a magnification at long times); arrows indicate the position  $t_1$  of the first dip that is ascribable to finite-size effects. Lower panel: curves correspond to different values of  $u$  and fixed  $L = 100$ .

Ising chain, when quenching from ground states in the disordered phase), in such a way to preserve translational invariance and to further reduce computational resources to a linear amount in  $L$ . We study the time behavior of the analogue, in fermionic language, of the transverse magnetization with either incoherent losses or pumping

$$S^{(l/p)}(t, g_0, g, u, L) = 2 \text{Tr}[\hat{c}_j^\dagger \hat{c}_j \rho(t)] - 1, \quad (36)$$

where the superscripts (l) and (p) refer to the loss or pumping dissipations related to the Lindblad operators (35). Note that the initial condition  $|\Phi_{g_0}\rangle$ , being the ground state of  $\hat{H}_K$ , can be interpreted as a state with a local fermionic filling given by  $n_j = \langle \Phi_{g_0} | \hat{c}_j^\dagger \hat{c}_j | \Phi_{g_0} \rangle$ , with  $n_j \in [0, 1]$ . For example, the extreme cases of disordered ground states are denoted by the completely filled state of fermions  $|\Phi_{+\infty}\rangle = |1, \dots, 1\rangle$  and the completely empty state of fermions  $|\Phi_{-\infty}\rangle = |0, \dots, 0\rangle$ .

In Fig. 10 we show some representative examples of the time dependence of the transverse magnetization when the system evolves according to the Lindblad equation (12) for  $g = 1$ . We start from the completely filled state corresponding to the ground state for  $g_0 \rightarrow +\infty$ , so that  $S(t=0) = 1$ . The dissipation is modeled in the form of particle losses, whose action is to deplete the system, and thus the value of  $S$  tends to generally decrease

in time. The upper panel displays the time behavior of  $S^{(l)}$  for different wire lengths  $L$  and fixed dissipation strength  $u = 0.1$ . With increasing  $L$ , the various curves overlap up to progressively longer times: for  $L \geq 20$  all of them appear to be identical up to  $t \lesssim 3$ , while looking at the curves for larger sizes  $L = 80$  and  $100$ , we see that they cannot be distinguished up to much longer times ( $t \approx 18$ ). This fact witnesses the existence of a well defined temporal behavior in the thermodynamic limit  $L \rightarrow \infty$ , as already pointed out for the unitary dynamics of a closed system (see Fig. 1). In fact, the emergence of dips and wiggles at finite size  $L$ , departing from the large- $L$  behavior and whose position progressively shifts to later times with increasing  $L$  (see arrows highlighting the first of such dips, clearly visible at the smallest available sizes), can be ascribed to finite-size effects, as we will see in Sec. IV C. Note also the emergence of an asymptotic stationary value  $S^{(l)}(t \rightarrow \infty) \approx -0.5$ , which weakly depends on the value of  $L$ , as hinted by the data reported in the inset. The bottom panel of Fig. 10 shows how the progressive increase of the dissipation strength  $u$  leads to a faster decay of  $S^{(l)}$  in time, down to the asymptotic behavior. This contrasts with the unitary case ( $u = 0$ ), where  $S$  converges to the large-time limit according to the oscillating behavior predicted by Eq. (18b).

Below we focus on all these issues in more detail, specifically addressing the thermodynamic limit behavior and finite-size corrections. As we shall see in the following analysis, some features characterizing the unitary evolution of the closed system disappear, while other will leave some residual trace.

## B. Behavior in the thermodynamic limit

Here we consider sufficiently large system sizes, so that finite-size effects are guaranteed not to play any role (i.e., for the times analyzed below, curves obtained for the two largest available values of  $L$  do overlap at any time). Note however that, due to the presence of dissipation, revivals are generally expected to be suppressed, and the influence of the boundary conditions to be less important than in closed systems. In practice, we carefully checked that chains of length  $L = 1000$  were sufficiently long to ensure that we are always probing the thermodynamic limit behavior (for example by comparing results for different sizes, and requiring agreement).

Analogously to closed systems, we define the thermodynamic limit of the transverse magnetization

$$\Sigma^{(l/p)}(t, g_0, g, u) \equiv S^{(l/p)}(t, g_0, g, u, L \rightarrow \infty), \quad (37)$$

When monitoring the time evolution of the transverse magnetization after a quench of the Hamiltonian parameter  $g$  and switching on the dissipation at  $t > 0$ , one finds a behavior of the type reported in Fig. 11:  $\Sigma^{(l/p)}$  starts from its corresponding value at the ground state with  $g_0$ , and then evolves in time until it converges to an asymptotic steady-state value, for  $t \rightarrow \infty$ . Comparing the

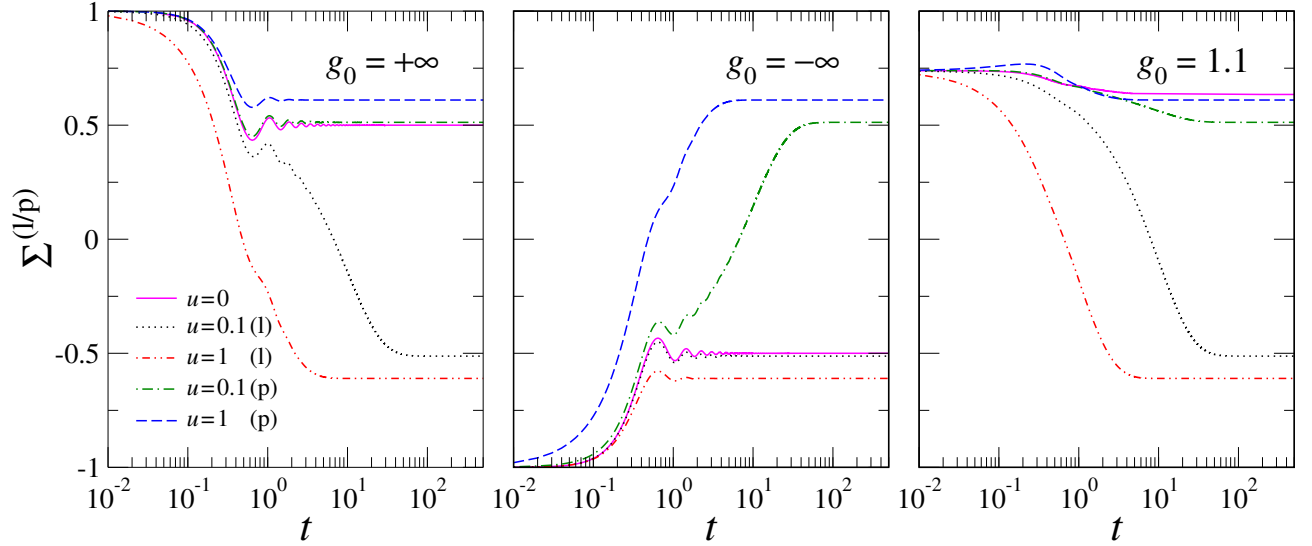


FIG. 11: Transverse magnetization as a function of time, in the dissipative Kitaev quantum wire quenched to the critical point  $g = 1$ . The three panels refer to different initial conditions, corresponding to: a completely filled state ( $g_0 = +\infty$ , left), a completely empty state ( $g_0 = -\infty$ , central), and a partially filled state ( $g_0 = 1.1$ , right). The dissipation is implemented in the form of either particle losses (l) or pumping (p), with two different strengths (see legend). The continuous purple line in each panel denotes the behavior in the absence of dissipation ( $u = 0$ ), cf. Eq. (14), which converges to  $F(g, g_0)$  for  $t \rightarrow \infty$  [see Eq. (17a)]. In all the curves reported here we have fixed  $L = 1000$ , after checking that such system size was sufficiently long to guarantee the study of time dependence in the thermodynamic limit. Times are in logarithmic scale, to better highlight the convergence to the  $t \rightarrow \infty$  stationary behavior.

three panels for different initial conditions, being either the completely filled, completely empty, or a partially filled state, we note that the steady-state magnetization  $\Sigma^{(l/p)}(t \rightarrow \infty)$  does not depend on such choice. This is a particular feature related to the presence of dissipation. Indeed the uniqueness of the (possibly existing) steady state has been proven for the loss and pumping operators [66–69]. This contrasts what happens in the absence of dissipation, where the surviving time-independent contribution  $F(g_0, g)$  clearly depends both on  $g$  and on  $g_0$  [see Eq. (17a) and the plateau reached at long times by the continuous purple lines in Fig. 11].

Notice however that, in the presence of incoherent pumping, the transverse magnetization evolves in time similarly to a closed system, which is initialized in the completely filled state  $|\Phi_{+\infty}\rangle$  (left panel). Conversely, with incoherent decay,  $\Sigma$  behaves similarly to a closed system initialized in the completely empty state  $|\Phi_{-\infty}\rangle$  (central panel). Asymptotic long-time values are also relatively close to the non-dissipative predictions given by  $F(\pm\infty, 1)$ , respectively. While the specific time dependence of  $\Sigma^{(l/p)}$  depends on the dissipation strength  $u$ , discrepancies with respect to the corresponding unitary behavior tend to amplify with increasing  $u$  (compare the continuous curves at  $u = 0.1$  with those at  $u = 1$ ), and even at  $u = 1$  it is possible to recognize a qualitatively similar trend. The above similarities between unitary and dissipative dynamics disappear when starting from a partially filled initial state  $|\Phi_{g_0, \text{with } |g_0| < \infty}\rangle$  (right panel).

As emerging from the data presented in Fig. 11, the

time evolution of the transverse magnetization satisfies

$$\Sigma^{(l)}(t, \pm\infty, g, u) = -\Sigma^{(p)}(t, \mp\infty, g, u), \quad (38)$$

when starting from one of the extremal states  $|\Phi_{\pm\infty}\rangle$  (compare left and central panels). The same holds for the unitary dynamics obtainable setting  $u = 0$ , i.e.  $\Sigma(t, +\infty, g, 0) = -\Sigma(t, -\infty, g, 0)$ . This is no longer the case if  $|g_0| < \infty$ . However, due to the independence on  $g_0$  of the steady-state value of  $\Sigma$ , we still have for fixed dissipation strength  $u$ :

$$\Sigma^{(l)}(t \rightarrow \infty, g_{0l}, g, u) = -\Sigma^{(p)}(t \rightarrow \infty, g_{0p}, g, u), \quad (39)$$

independently of the values  $g_{0l}$  and  $g_{0p}$ .

We stress that, while the figure only reports results for quenches ending at the critical point  $g = g_c = 1$ , analogous conclusions on the steady-state values and symmetry properties of the model can be drawn for generic values of  $g$  (not shown here).

To better analyze the influence of dissipation and of the post-quench transverse field  $g$  on the long-time value of the transverse magnetization, in Fig. 12 we report the dependence of  $\Sigma^{(p)}(t \rightarrow \infty)$  on  $g$ , for two distinct values of incoherent pumping strength  $u$ . These are compared with the unitary prediction given by  $F(+\infty, g)$  [cf. Eq. (18a)]. As is visible, the discontinuity in the first derivative at  $g_c$  is smeared by the coupling with the environment. For small  $u$  it is however possible to recover a signal of singularity in  $g_c$ . In the figure we did not report the case of incoherent decay, being equal to the

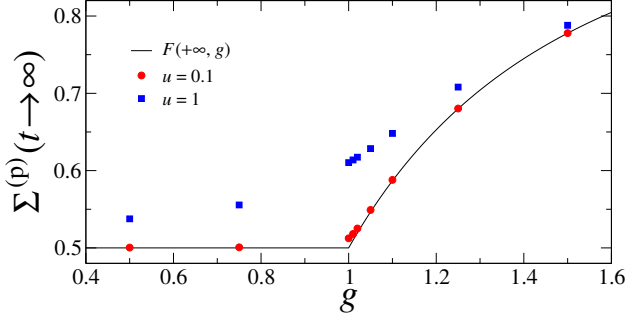


FIG. 12: Asymptotic long-time value reached by the transverse magnetization,  $\Sigma^{(p)}(t \rightarrow \infty)$ , as a function of the post-quench value of  $g$  in the presence of incoherent pumping of strength  $u = 0.1$  (red circles) and  $u = 1$  (blue squares). The continuous black line is the function  $F(+\infty, g)$  of Eq. (18a) for the large-time limit in the absence of dissipation and starting from  $g_0 = +\infty$ .

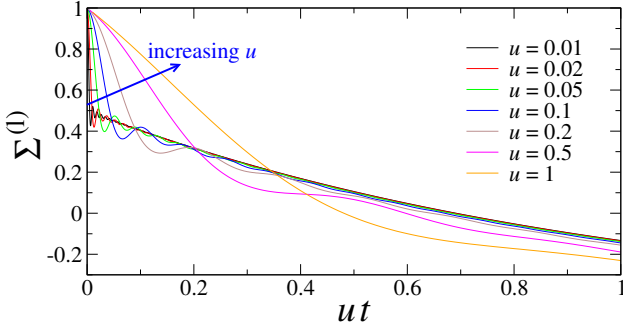


FIG. 13: Scaling behavior of  $\Sigma^{(l)}$  in the presence of incoherent particle losses, for a quench from  $g_0 = +\infty$  to  $g = 1$ . The various curves are for different values of  $u$  (see legend) and  $L = 1000$ , so to ensure having reached the behavior in the thermodynamic limit. Times have been rescaled according to the adimensional variable  $\nu = ut$ .

opposite value of pumping [see Eq. (39)] and matching the corresponding unitary prediction  $F(-\infty, g)$ .

We conclude this part by observing that, in the large time-limit, the time evolution of the transverse magnetization, for small dissipation strength  $u \ll 1$ , obeys an asymptotic scaling behavior of the form

$$\Sigma^{(l/p)}(t, g_0, g, u) \approx \Sigma_r^{(l/p)}(g_0, g, \nu), \quad \nu \equiv ut, \quad (40)$$

keeping  $\nu$  fixed. The data in Fig. 13, for various values of the strength  $u$  of incoherent losses, nicely support this behavior (note also that, for  $u \gtrsim 0.1$ , the collapse of the various curves definitely becomes less accurate). An analogous data collapse is seen in the case of incoherent particle pumping. We stress that the scaling behavior put forward in Eq. (40) should not be considered as unexpected, since the parameter  $u$  plays the role of decay rate of the dissipation.

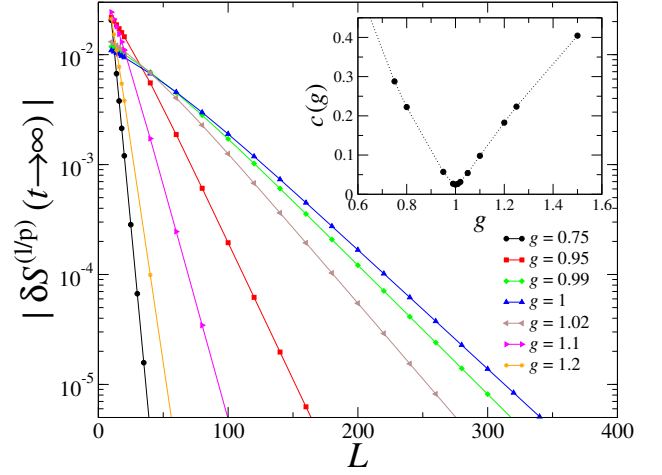


FIG. 14: The difference  $\delta S^{(l/p)}$ , cf. Eq. (41), in the asymptotic long-time limit, between the transverse magnetization at finite length  $L$  and the corresponding thermodynamic limit value for  $L \rightarrow \infty$ . The various curves are for different values of  $g$  and for fixed dissipation strength  $u = 0.1$ . These data are unaffected by the choice of dissipation (being either losses or pumping) and of  $g_0$ . The inset shows the exponential decay rate of such discrepancy, as a function of  $g$ .

### C. Finite-size effects

As for the case of closed systems, we now focus on finite-size effects for PBC and look at the difference

$$\delta S^{(l/p)}(t, g_0, g, u, L) = S^{(l/p)}(t, g_0, g, u, L) - \Sigma^{(l/p)}(t, g_0, g, u), \quad (41)$$

where  $\Sigma^{(l/p)}(t, g_0, g, u)$  is the infinite-size limit of  $S^{(l/p)}(t, g_0, g, u, L)$ . Figure 14 displays such difference in the asymptotic long-time limit for a prototypical dissipative situation, where the system is quenched to the critical point  $g_c$  and with dissipation strength  $u = 0.1$ . As noted before, the value reached by  $\delta S$  in the long-time stationary regime does not depend on  $g_0$  and on the type of dissipation (losses or pumping). The various curves show that  $\delta S^{(l/p)}$  decays exponentially in the large- $L$  limit, i.e.

$$\delta S^{(l/p)}(t \rightarrow \infty) \sim e^{-c(g)L}. \quad (42)$$

It is also interesting to note that the exponential rate  $c(g)$  displays a minimum at  $g = g_c = 1$ , thus signaling the emergence of larger finite-size corrections at the critical point (although they are still exponentially suppressed).

Coming back to the time behavior of  $S^{(l)}(t)$  at finite size, shown in the upper panel of Fig. 10, we can observe a dip (and subsequent wiggles) at larger and larger times  $t_1$  with increasing  $L$ , so that  $t_1 \sim L$  (see the inset of Fig. 15). This finite-size behavior apparently resembles the one already observed in closed systems, as in Fig. 1. However, a closer inspection of the scaling of the height of such dips reveals that their depth is exponentially suppressed with increasing  $L$ , as clearly visible from the data

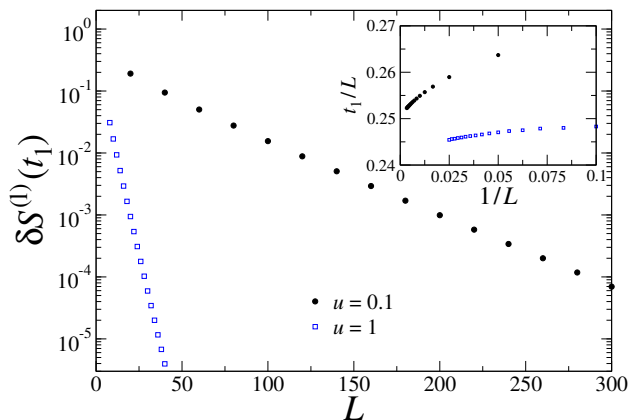


FIG. 15: Scaling behavior of the first dip (see arrows in Fig. 10) corresponding to finite-size effects in the transverse magnetization, for a quench from  $g_0 = +\infty$  to  $g = 1$  and in the presence of incoherent losses of strength  $u = 0.1$ . The main frame displays the value of the subtracted magnetization at the dip,  $\delta S^{(1)}(t_1)$  [cf. Eq. (41)], as a function of  $L$  in semilog scale. The inset displays the position of the dip  $t_1/L$  vs.  $1/L$ .

shown in the main frame of Fig. 15. The large- $L$  limit is thus approached much faster than for the unitary dynamics (compare, e.g., with Fig. 5). We checked that these facts are not qualitatively affected by the choice of the pre- and post-quench values  $g_0$  and  $g$ , nor by the type and the strength of dissipation.

In conclusion we observe that, differently from the unitary dynamics of closed systems, the presence of dissipation dramatically reduces finite-size effects and no relevant revival phenomena emerge, as substantially expected.

## V. QUENCHES FROM THE ORDERED STATE

We now address quenches of the quantum Ising chain (4) starting from a completely ordered state (i.e., a fully magnetized state  $|\Psi(t=0)\rangle = |\uparrow, \dots, \uparrow\rangle$ ). This corresponds to one of the degenerate ground state in thermodynamic limit when  $g_0 \rightarrow 0$ , obtainable by the ground state in the limit

$$|\Psi(0)\rangle = \lim_{g_0 \rightarrow 0} \lim_{h \rightarrow 0^+} \lim_{L \rightarrow \infty} |\text{GS}\rangle, \quad (43)$$

where  $h$  is an external homogenous magnetic field coupled to the longitudinal magnetization. Since such initial state breaks the  $\mathbb{Z}_2$  symmetry (5) of the model, one finds a nonzero longitudinal magnetization  $M$  [cf. Eqs. (6a) and (7)] along the quantum evolution (1) after quenching the transverse field parameter  $g$ . We will not explicitly show data for initial partially ordered states (i.e., corresponding to finite values of  $0 < g_0 < 1$ ), since the same conclusions apply also in such circumstances. Therefore, in the following we drop the dependence on  $g_0$  of the observables.

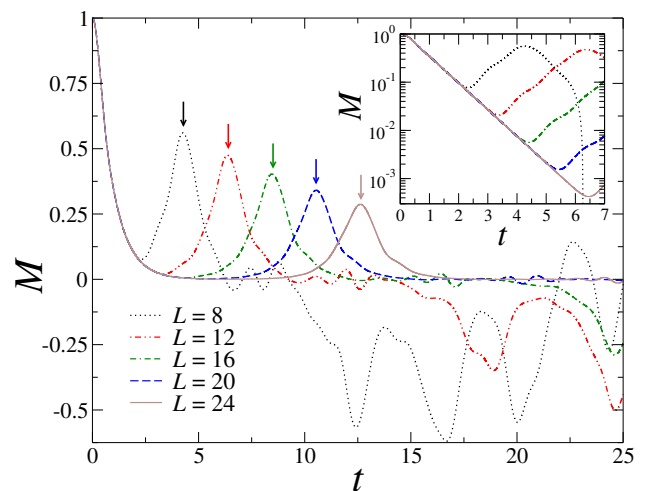


FIG. 16: Longitudinal magnetization after a quench in the quantum Ising chain with PBC, starting from the symmetry-broken ordered state at  $g_0 = 0$ , to  $g = 1$ . The various data sets are for different chain lengths; arrows denote the position of the first peak emerging in the finite-size revivals, located at time  $t_1(L) \approx L/(2v_m)$ . The inset is a magnification at small times in semilog scale, showing that, in the thermodynamic limit, the magnetization decays exponentially with  $t$ .

An example of the evolution of  $M(t)$  after the above protocol is provided by Fig. 16, where we focus on quenches to the critical point  $g = g_c = 1$  for different lattice sizes  $L$ . Similarly to the case of quenches from disordered states, the small-time behavior appears to be independent of the size (see, e.g., Fig. 1), and in this case it drops exponentially in time. Then, after some time which depends on  $L$  and on the choice of the boundary conditions, a non monotonic behavior related to finite-size revival effects sets in, as we shall clarify below.

At this stage it is important to stress that, for quenches from ordered states ( $g_0 < 1$ ), one cannot exploit the exact mapping with the quantum fermionic wires (23) with ABC. Therefore in this case, to study the exact out-of-equilibrium behavior of the system, we are forced to employ exact-diagonalization methods which typically scale exponentially with  $L$  and thus severely limit the simulatable lattice sizes up to  $L \simeq 24$ . In passing we mention that a new formalism based on the correspondence between momentum space and real space has been recently put forward in Ref. [70], which would enable to evaluate the longitudinal magnetization for considerably larger system sizes, by numerically computing suitable Pfaffians. Nonetheless, as we shall see in a moment, brute-force diagonalization will be sufficient to infer the main dynamical features we are interested in.

### A. Quenches in the thermodynamic limit

We first discuss the thermodynamic limit of the longitudinal magnetization  $M(t)$ . For the transverse magne-

tization  $S(t)$ , it is sufficient to take the limit  $g_0 \rightarrow 0$  of the exact analytic formulas reported in Sec. III A.

The longitudinal magnetization in the thermodynamic limit,

$$\mathcal{M}(t, g) \equiv M(t, g, L \rightarrow \infty), \quad (44)$$

turns out to vanish in the large-time limit  $t \rightarrow \infty$ . Indeed it presents an asymptotic exponential decay, according to [20]

$$\mathcal{M}(t, g) \approx \mathcal{M}_a(t, g) = A(g) \exp[-\Gamma(g) t], \quad (45)$$

where

$$A(g) = \frac{1}{\sqrt{2}} \left[ 1 + \sqrt{1 - g^2} \right]^{1/2}, \quad (46)$$

$$\Gamma(g) = \int_0^\pi \frac{dk}{\pi} 2 \frac{g \sin(k)}{\Lambda(g, k)} \ln \left[ \frac{1 - g \cos(k)}{\Lambda(g, k)} \right], \quad (47)$$

where  $\Lambda(g, k)$  is the function reported in Eq. (16) setting  $\gamma = 1$ . The asymptotic behavior (45) was derived essentially for  $g < 1$  in Ref. [20]. Similarly as for the transverse magnetization [see Eq. (20)], even in this case we note a singular behavior at  $g = g_c = 1$ . Indeed, around  $g_c$ , the decay function  $\Gamma(g)$  behaves as

$$\Gamma(g) = \begin{cases} 4/\pi - 2\sqrt{2(1-g)} + O(1-g) & \text{for } g < 1, \\ 4/\pi & \text{for } g \geq 1. \end{cases} \quad (48)$$

We have carefully checked that these asymptotic analytic behaviors are supported by our data (not shown).

A noteworthy issue is the fact that numerical results evidence a discontinuity at  $g = g_c = 1$  also in the prefactor  $A(g)$ . As a matter of fact, while for  $g \neq 1$  the formula (46) appears to be correct, the value  $A(1)$  which captures the long-time behavior of  $M$  is not provided by the  $g \rightarrow 1$  limit of Eq (46). Indeed, as explicitly reported in Fig. 17, we found that

$$A(1) \approx 1.229 \quad (49)$$

(with an accuracy of about two per mille), definitely different from the prefactor predicted by Eq. (46), i.e.  $A(1) = 1/\sqrt{2} \approx 0.707$ . This signals a discontinuity in the prefactor of Eq. (45) of the asymptotic large-time behavior, indicating that such an asymptotic behavior is not uniformly approached for  $g \rightarrow 1^-$ . In particular, the analytic estimate with  $A(1)$  given by Eq. (49) is nearly indistinguishable from the numerical data, thus demonstrating convergence for times sufficiently small to ensure the reaching of the thermodynamic limit for the largest available size (compare the continuous black line with the dot-dashed red line). A closer look at the relative discrepancies shows that, in fact, the exact solution presents an oscillating contribution that vanishes at long times (see inset). On the other hand, the estimate provided by Eq. (46) does not provide the correct result (dashed blue line).

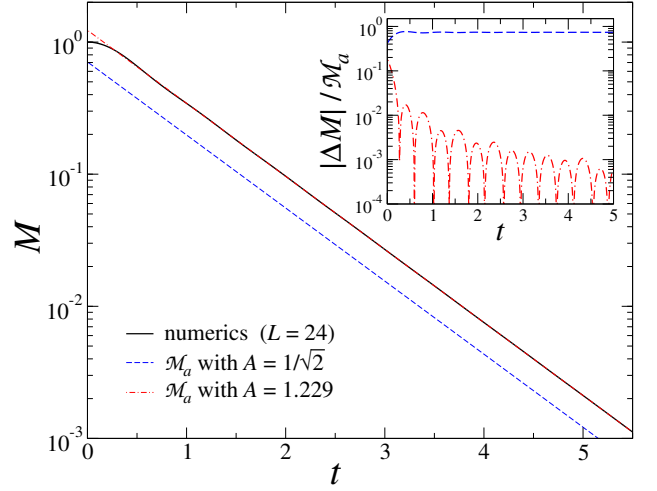


FIG. 17: Longitudinal magnetization  $M(t)$  in the Ising chain for a quench from the completely ordered state to  $g = 1$ . These analytical and numerical results are supposed to show the behavior in the thermodynamic limit. In particular, the continuous black curve is the result of a numerical simulation with  $L = 24$  sites; we checked that such system size guarantees the study of time dependence in the thermodynamic limit, up to time  $t = 5.5$ . Dashed blue and dot-dashed red data sets respectively denote the predictions  $\mathcal{M}(t, 1)$  given by Eq. (45) with either  $A(1)$  in Eq. (46) or with  $A(1) = 1.229$ . The inset shows the relative difference  $|\Delta\mathcal{M}(t, 1)|/\mathcal{M}_a(t, 1)$ , where  $\Delta\mathcal{M}(t, g) = \mathcal{M}(t, g) - \mathcal{M}_a(t, g)$  as a function of time, for the two predictions discussed before.

Let us now have a closer look at the infinite-size limit of the longitudinal magnetization as a function of the time after the quench, for some different values of  $g$ , starting from the completely ordered state at  $g_0 = 0$ . To infer the thermodynamic-limit behavior we first performed numerical simulations at various lattice sizes, up to  $L = 24$ . For sufficiently small values of  $t$ , the curves at the largest available sizes superimpose, therefore they can be considered as a good approximation of the thermodynamic large- $L$  limit (see Fig. 16 for an example at  $g = 1$ ). The complete  $L \rightarrow \infty$  curve has been then reconstructed by matching with the analytical asymptotic results discussed above. Such curves are reported in Fig. 18. We note that, when crossing the critical point  $g = g_c = 1$ , they become nonmonotonic and start oscillating, showing a negative dip. This may be considered as a particular signature of the transition point.

We finally mention that Refs. [18, 22] exploit a semiclassical framework to compute the longitudinal magnetization and related correlations. This semiclassical approach provides reliable results in regions of the Hamiltonian parameters, where a quasi-particle picture based on kinks or domain walls turns out to be effective, for example for small values of the transverse field  $g$ .



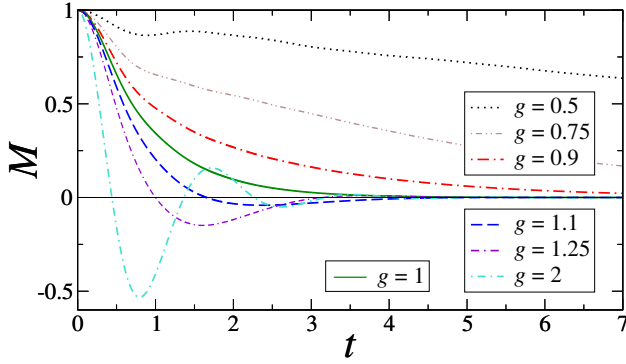


FIG. 18: Time dependence of the longitudinal magnetization in the thermodynamic limit, up to time  $t = 7$ , after quenches to various values of  $g$ , starting from the fully ordered state.

### B. Finite-size effects with PBC

To analyze finite-size effects, we consider again the subtracted quantity  $\delta S$  defined in Eq. (24), and the corresponding  $\delta M$  for the longitudinal magnetization

$$\delta M(t, g, L) \equiv M(t, g, L) - \mathcal{M}(t, g). \quad (50)$$

Since, for the latter, we do not have the exact large- $L$  curve but only its large-time exponential behavior  $\mathcal{M}_a$ , to evaluate  $\mathcal{M}(t, g)$  we use both numerical results for the largest lattice sizes supplemented by their asymptotic large-time behavior, as mentioned at the end of Sec. V A.

To begin with, we present results for quenches to the critical point  $g = g_c = 1$ . Even in the case of quenches starting from ordered states, the transverse magnetization behaves consistently with Eq. (25), which explains the finite-size scaling behavior of the main features of the time dependence, such as the relevant time scaling variable  $t_L \equiv t/L$ , the revival features starting at  $t_k = kL/(2v_m)$ , and the  $L^{-1/3}$  power law of the envelope of the short time oscillations. This is witnessed by the curves plotted in the upper panel of Fig. 19, which analyze the behavior of the transverse magnetization  $\delta S$  after a quench from the perfectly ordered state at  $g_0 = 0$ , to the critical point  $g = g_c = 1$ . Note the appearance of a good data collapse already at  $L \lesssim 24$ , after the proper rescaling as predicted in (25) using  $a = 1/3$  and  $t_L = t/L$ .

In the lower panel of the same figure we report data of the subtracted longitudinal magnetization  $\delta M$  [cf. Eq. (50)], for the same type of quench from the symmetry-broken state at  $g_0 = 0$ . The subtraction of the asymptotic large-time behavior in the thermodynamic limit is effective, indeed we clearly observe a relatively large interval ( $t/L \approx 0.2$ , in the figure) where the time dependence appears flat and vanishing. As expected, the positions of the peaks and dips confirm that the relevant time scaling variable is  $t_L = t/L$ , analogously as for the transverse magnetization (not shown). However, the behavior of the maxima/minima at the peaks/dips suggests a different rescaling, as can be seen from the data for the

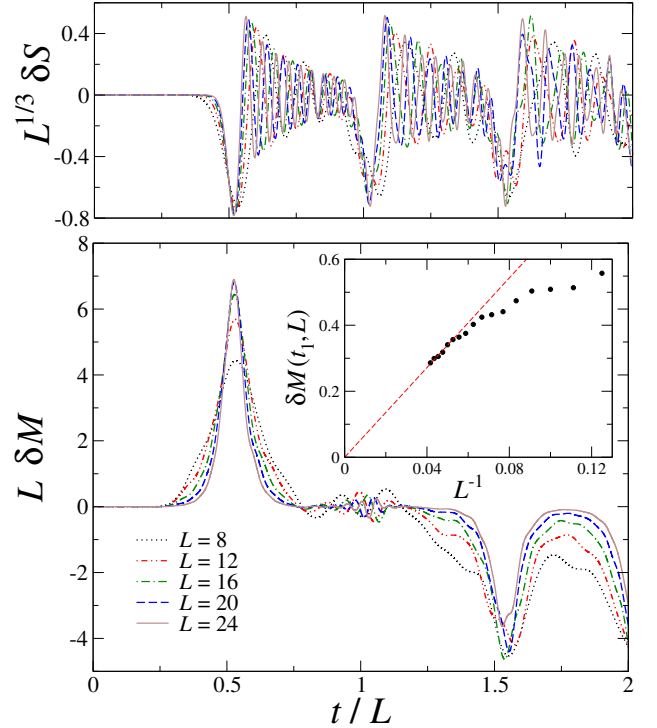


FIG. 19: Time behavior of the transverse (upper panel) and longitudinal (lower panel) magnetization after a quench from the symmetry-broken state at  $g_0 = 0$ , to  $g = 1$ . Times have been rescaled with  $t/L$  and subtracted magnetizations as  $L^{1/3} \delta S$  and  $L \delta M$ , respectively [cf. Eqs. (24) and (50)]. The different data sets are for systems with PBC and various chain lengths, as indicated in the legend. The inset in the lower panel shows data for  $\delta M(t_1, L)$  vs.  $L^{-1}$ ; the dashed red line is a linear fit for  $L \geq 20$ , assuming the prediction of Eq. (51) with  $\omega = 1$ .

magnetization values at the first peak vs. the inverse size  $L^{-1}$ , shown in the inset. Therefore, despite the impossibility to reach higher sizes with great accuracy prevents us from giving a conclusive statement, our data hint at the following finite-size scaling behavior

$$\delta M(t, g = 1, L) \approx L^{-c} f_s(t_L), \quad c \approx 1, \quad (51)$$

in accordance with the nice approach to data collapse, for the curves with  $L \lesssim 24$  shown in the main frame of the lower panel, reporting the rescaled magnetization  $L \delta M$  vs. the rescaled time  $t/L$ .

The above asymptotic large- $L$  features are also observed in quenches to values of  $g$  different from  $g_c = 1$ , in particular around it. On the other hand, as shown in Fig. 20, the situation is less clear for small values of  $g$ ; see e.g. the case of  $g = 0.5$ , where the data for different values of  $L$  appear to tend to the same value  $M \approx 0.8$ . Of course, this may reflect a slow convergence in the chain size; in other words, the approach to an asymptotic behavior such as that reported in Eq. (51) may be significantly delayed for quenches to small values of  $g$ . Large lattice sizes would be necessary to clarify this point.

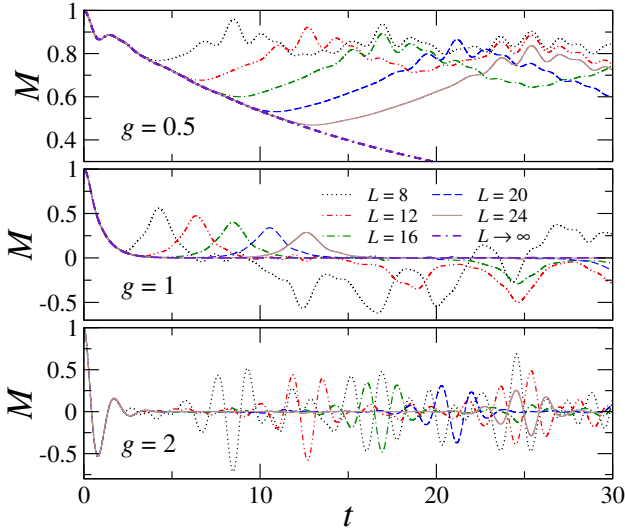


FIG. 20: Longitudinal magnetization as a function of time, after quenches to various values of  $g$  in the ordered phase ( $g = 0.5$ , upper panel), at the critical point ( $g = 1$ , central panel), and in the disordered phase ( $g = 2$ , bottom panel), starting from the fully ordered state. The various curves are for different chain lengths, as reported in the legend.

### C. Finite-size effects with OBC

Let us finally consider the role of OBC for quenches starting from the symmetry-broken phase. The decay of the longitudinal magnetization as a function of the position, and in particular at the boundaries, was discussed in Ref. [17]. Here we only explicitly discuss central magnetizations, for time evolutions controlled by the critical Hamiltonian ( $g = 1$ ) and starting from the fully ordered state ( $g_0 = 0$ ). Data for the subtracted transverse and longitudinal magnetization, respectively given by Eqs. (29) and by the analogous of Eq. (50) for  $M_c$ ,

$$\delta M_c(t, g, L) \equiv M_c(t, g, L) - \mathcal{M}_c(t, g), \quad (52)$$

are reported in Fig. 21. Of course, the large- $L$  thermodynamic limit is expected to be the same as for  $S$  and  $M$ . This is confirmed by the results shown in the two upper panels of the figure, where a plateau equal to zero is clearly visible for short times  $t/L \lesssim 0.2$ . The scaling of first large dip with the size is compatible with what we already observed for PBC (i.e. same scaling with  $L$ , as witnessed by the data in the bottom panel), cf. Eq. (51).

## VI. QUENCHES IN THE ANNNI MODEL

We now extend our study to Ising-like systems in the presence of integrability-breaking perturbations. For this purpose, we consider quantum quenches in the anisotropic next-nearest neighbor Ising (ANNNI) chain, changing the quench parameter across an underlying

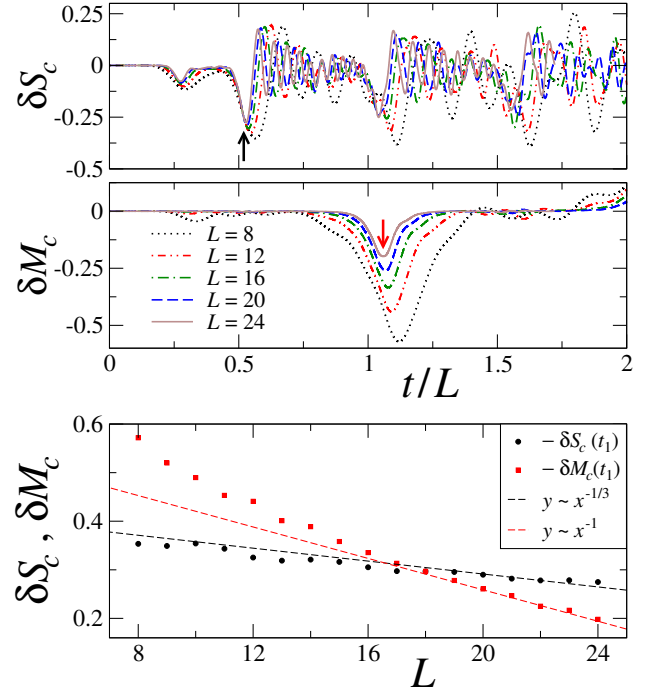


FIG. 21: Subtracted transverse (upper panel) and longitudinal (central panel) magnetization after a quench starting from the symmetry-broken state at  $g_0 = 0$ , to  $g = 1$ , calculated at the center of an Ising chain with OBC. Data are plotted as a function of the rescaled time  $t/L$ . The lower panel shows  $\delta S_c(t_1)$  and  $\delta M_c(t_1)$  vs.  $L$ ; the dashed lines indicate the behaviors  $\delta S_c(t_1) \sim L^{-1/3}$  (black set) and  $\delta M_c(t_1) \sim L^{-1}$  (red set), respectively.

quantum phase transition. Its Hamiltonian reads

$$\hat{H}_{\text{ANNNI}} = -J \sum_{x=1}^L \left[ \hat{\sigma}_x^{(1)} \hat{\sigma}_{x+1}^{(1)} - \kappa \hat{\sigma}_x^{(1)} \hat{\sigma}_{x+2}^{(1)} + g \hat{\sigma}_x^{(3)} \right]. \quad (53)$$

For values of  $\kappa$  sufficiently small, quantum ANNNI models present a continuous Ising-like transition, see e.g. Refs. [51, 71] and references therein.

In the following we analyze quench protocols starting from the fully ordered state (corresponding to  $g \rightarrow 0$ ) to the critical parameter  $g = g_c(\kappa)$  [71, 72]. Figure 22 displays some results for  $\kappa = 0.15$ , for which [71]  $g_c = 0.73405(4)$ . They look qualitatively similar to those obtained for the Ising chain ( $\kappa = 0$ ), see Fig. 1. The results up to  $L = 24$  allow us to determine the quantum evolution  $\mathcal{M}(t, \kappa, g)$  in the thermodynamic limit up to  $t \approx 7$ , by checking their convergence with increasing  $L$ , see Fig. 23. The resulting curves in the thermodynamic limit are shown in Figs. 23.

We note remarkable similarities with the case of the Ising chain ( $\kappa = 0$ ), in particular the qualitative different behavior of the evolution of the longitudinal magnetization when quenching to the ordered and disordered phases. Indeed quenches within the ordered phase,  $g < g_c$ , are characterized by exponential decays to zeroes,

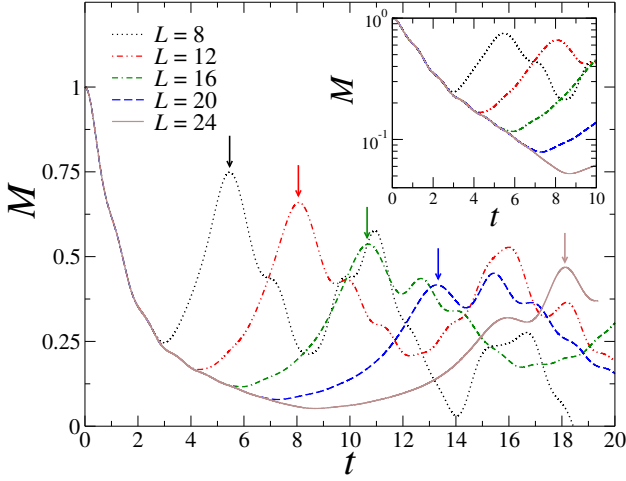


FIG. 22: Same as in Fig. 16, but for the post-quench critical dynamics of the nonintegrable ANNNI chain with PBC and  $\kappa = 0.15$ . Here we set  $g = g_c(\kappa = 0.15) = 0.73405(4)$  [71].

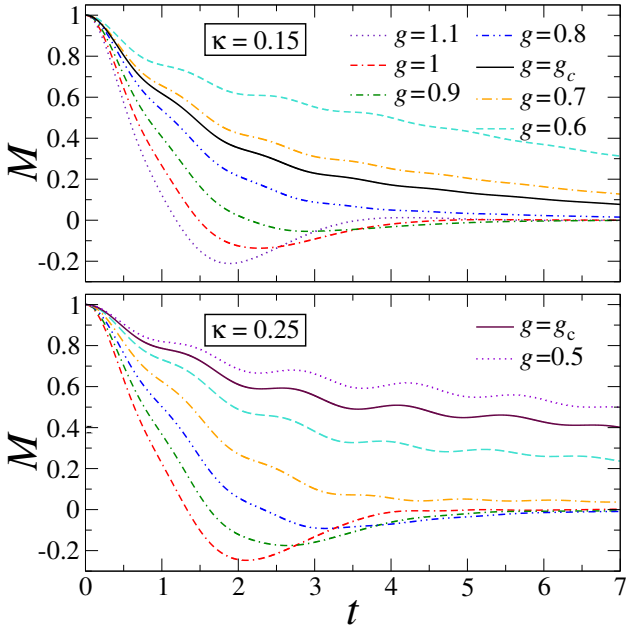


FIG. 23: Same as in Fig. 18, but for the ANNNI chain with PBC and  $\kappa = 0.15$  (top) and  $\kappa = 0.25$  (bottom). We recall that  $g_c = 0.73405(4)$  for  $\kappa = 0.15$  and  $g_c = 0.5403(3)$  for  $\kappa = 0.25$ .

while quenches to the disordered phase,  $g > g_c$ , show minima, so that the asymptotic vanishing value gets approached from below. The behavior around  $g = g_c$  turns out to be less clear, requiring further and more accurate numerical studies. This shows that these qualitative features may persist even in nonintegrable models. They provide different characterizations of the different phases, which may turn useful to distinguish different phases within hard quenching protocols. Further studies are deemed in order to understand whether such qualitative differences can be also used to obtain accurate

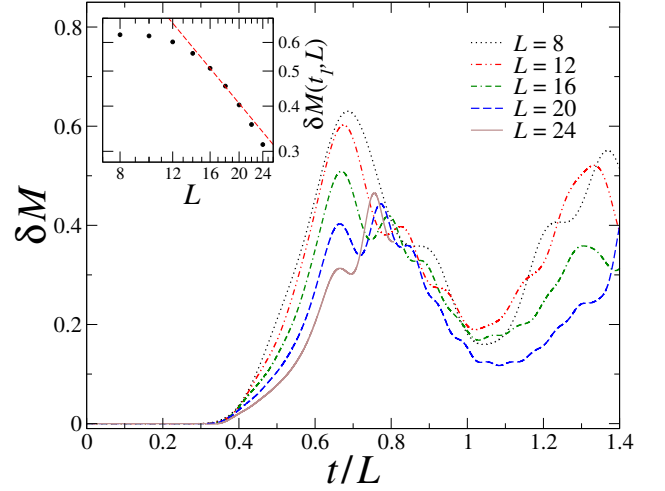


FIG. 24: Subtracted longitudinal magnetization after a quench in the ANNNI chain with PBC and  $\kappa = 0.15$ , from the symmetry-broken state at  $g_0 = 0$ , to  $g = g_c$ . Data for different system sizes are plotted a function of the rescaled time  $t/L$ . The inset shows the value of the subtracted magnetization at the first peak,  $\delta M(t_1)$ , vs.  $L$ ; the dashed line indicates the behavior  $\delta M(t_1) \sim L^{-1}$ .

estimates of the transition point.

Our analysis substantially supports the idea that the quench dynamics may be employed to signal the presence of phase transitions even in nonintegrable systems, as also put forward in Ref. [51], where the peculiar behaviors of some local observables at intermediate times after quenches were investigated for the purpose of locating the phase transition.

Finally, Fig. 24 displays the subtracted quantity

$$\delta M(t, \kappa, g, L) \equiv M(t, \kappa, g, L) - \mathcal{M}(t, \kappa, g). \quad (54)$$

for  $\kappa = 0.15$  and for a quench to  $g = g_c$ . Again the behavior is quite similar to that observed for the Ising chain; in particular, the position of the first peak scales as  $t_L \equiv t/L$ . As highlighted in the inset, while the reported data cannot be considered conclusive due to the small simulatable system sizes, the decay of  $\delta M(t_1)$  is consistent with an asymptotic  $L^{-1}$  behavior, as for the scaling ansatz reported in Eq. (51).

## VII. CONCLUSIONS

We have investigated the out-of-equilibrium dynamics of one-dimensional quantum Ising-like systems arising from quenches of the Hamiltonian parameter  $g$  driving the phase transition that separates the quantum paramagnetic and ferromagnetic phases. To this purpose, we have considered the simplest quenching protocol: the system starts from the ground state of the many-body Hamiltonian associated with a given value  $g_0$  of the parameter; the latter is then suddenly changed to  $g \neq g_0$ .

The resulting quantum evolution is driven either by the unitary dynamics (1), for a closed system, or by the Lindblad equation (12), in the presence of dissipative interactions with an environment. The issue we have addressed is whether, and how, quantum transitions can be probed by the study of such quench protocols.

The behavior of the transverse and longitudinal magnetizations have been considered both in the infinite-size limit and also considering finite-size effects, for systems with periodic and open boundary conditions. The out-of-equilibrium evolution of such magnetizations in quantum XY chains, in the thermodynamic limit, cf. Eq. (3), develops a singular dependence on the quench parameter  $g$  around its critical value  $g_0$ , for any anisotropy parameter  $\gamma > 0$  and starting point  $g_0$ , including the extremal ones corresponding to fully disordered and ordered initial states. Similar singularities have been reported in Ref. [47]. Finite-size effects, related to revival phenomena, develop peculiar scaling laws characterized by power laws. Their exponents have been accurately determined numerically, suggesting simple fractions, see e.g. Eqs. (25) and (51) for the transverse and the longitudinal magnetizations, respectively. Such power laws are not actually related to the quantum transitions, since they are observed in generic quenches even those not involving critical parameters. They should be related to the interference of quasi-particle excitations after traveling across the finite chain. The understanding of such

emerging power laws deserve further investigations.

Finally we have analyzed the effects of two different mechanisms moving Ising-like systems away from integrability, by adding either dissipation or further nonintegrable Hamiltonian terms (such as those of the ANNNI models). In the case of system-bath couplings, modeled by a Lindblad equation with local decay and pumping dissipation operators within the fermionic model obtainable by a Jordan-Wigner mapping, the singularity of the time evolution of the transverse magnetization in quenches from disordered states to the critical Hamiltonian is washed out. Moreover, local dissipation suppresses finite-size effects exponentially, in particular the revival phenomena observed in closed systems. On the other hand, our analysis of the ANNNI model reveals that some of the main features of the post-quench dynamics persist, in particular the evolution of the longitudinal magnetization shows qualitative differences when the quenches are performed within the ordered phase or crossing the transition point toward the disordered phase. Therefore, as already hinted in Ref. [51], hard quench protocols may be exploited to get evidence of phase transitions even in nonintegrable systems.

It would be tempting to test whether phenomena similar to those observed here may emerge also for other classes of quantum transitions, which include different universality classes or topological phase transitions.

- 
- [1] I. Bloch, Quantum coherence and entanglement with ultracold atoms in optical lattices, *Nature* **453**, 1016 (2008).
  - [2] I. M. Georgescu, S. Ashhab, and F. Nori, Quantum simulation, *Rev. Mod. Phys.* **86**, 153 (2014).
  - [3] M. Greiner, O. Mandel, T. Esslinger, T. W. Hänsch, and I. Bloch, Quantum phase transition from a superfluid to a Mott insulator in a gas of ultracold atoms, *Nature* **415**, 39 (2002).
  - [4] T. Kinoshita, T. Wenger, and D. S. Weiss, A quantum Newton's cradle, *Nature* **440**, 900 (2006).
  - [5] S. Hofferberth, I. Lesanovsky, B. Fischer, T. Schumm, and J. Schmiedmayer, Non-equilibrium coherence dynamics in one-dimensional Bose gases, *Nature* **449**, 324 (2007).
  - [6] S. Trotzky, Y.-A. Chen, A. Fleisch, I. P. McCulloch, U. Schollwöck, J. Eisert, and I. Bloch, Probing the relaxation towards equilibrium in an isolated strongly correlated one-dimensional Bose gas, *Nat. Phys.* **8**, 325 (2012).
  - [7] M. Cheneau, P. Barmettler, D. Poletti, M. Endres, P. Schaub, T. Fukuhara, C. Gross, I. Bloch, C. Kollath, and S. Kuhr, Light-cone-like spreading of correlations in a quantum many-body system, *Nature* **481**, 484 (2012).
  - [8] M. Gring, M. Kuhnert, T. Langen, T. Kitagawa, B. Rauer, M. Schreitl, I. Mazets, D. Adu Smith, E. Demler, and J. Schmiedmayer, Relaxation and Prethermalization in an Isolated Quantum System, *Science* **337**, 1318 (2012).
  - [9] Th. Niemeijer, Some exact calculations on a chain of spins 1/2, *Physica* **36**, 377 (1967); Some exact calculations on a chain of spins 1/2 II, *Physica* **39**, 313 (1968).
  - [10] E. Barouch, B. M. McCoy, and M. Dresden, Statistical mechanics of the XY model. I, *Phys. Rev. A* **2**, 1075 (1970).
  - [11] G. De Chiara, S. Montangero, P. Calabrese, and R. Fazio, Entanglement entropy dynamics of Heisenberg chains, *J. Stat. Mech.* P03001 (2006).
  - [12] M. Rigol, V. Dunjko, V. Yurovsky, and M. Olshanii, Relaxation in a Completely Integrable Many-Body Quantum System: An Ab Initio Study of the Dynamics of the Highly Excited States of 1D Lattice Hard-Core Bosons, *Phys. Rev. Lett.* **98**, 050405 (2007).
  - [13] M. Rigol, V. Dunjko, and M. Olshanii, Thermalization and its mechanism for generic isolated quantum systems, *Nature* **452**, 854 (2008).
  - [14] M. Žnidarič, T. Prosen, and P. Prelovšek, Many-body localization in the Heisenberg XXZ magnet in a random field, *Phys. Rev. B* **77**, 064426 (2008).
  - [15] T. Prosen and M. Žnidarič, Matrix product simulations of non-equilibrium steady states of quantum spin chains, *J. Stat. Mech.* (2009) P02035.
  - [16] A. Polkovnikov, K. Sengupta, A. Silva, and M. Vengalattore, Colloquium: Nonequilibrium dynamics of closed interacting quantum systems, *Rev. Mod. Phys.* **83**, 863 (2011).
  - [17] F. Igloi and H. Rieger, Quantum Relaxation after a Quench in Systems with Boundaries, *Phys. Rev. Lett.* **106**, 035701 (2011).

- [18] H. Rieger and F. Iglói, Semiclassical theory for quantum quenches in finite transverse Ising chains, *Phys. Rev. B* **84**, 165117 (2011).
- [19] A. Gambassi and A. Silva, Large Deviations and Universality in Quantum Quenches, *Phys. Rev. Lett.* **109** 250602 (2012).
- [20] P. Calabrese, F. H. L. Essler, and M. Fagotti, Quantum quench in the transverse field Ising chain: I. Time evolution of order parameter correlators, *J. Stat. Mech.* (2012) P07016.
- [21] P. Calabrese, F. H. L. Essler, and M. Fagotti, Quantum quenches in the transverse field Ising chain: II. Stationary state properties, *J. Stat. Mech.* (2012) P07022.
- [22] B. Blass, H. Rieger, and F. Iglói, Quantum relaxation and finite size effects in the XY chain in a transverse field after global quenches, *Eur. Phys. Lett.* **99**, 30004 (2012).
- [23] J.-S. Caux and F. H. L. Essler, Time evolution of local observables after quenching to an integrable model, *Phys. Rev. Lett.* **110**, 257203 (2013).
- [24] M. Fagotti, M. Collura, F. H. L. Essler, and P. Calabrese, Relaxation after quantum quenches in the spin-1/2 Heisenberg XXZ chain, *Phys. Rev. B* **89**, 125101 (2014).
- [25] R. Nandkishore and D. A. Huse, Many body localization and thermalization in quantum statistical mechanics, *Annu. Rev. Condens. Matter Phys.* **6**, 15 (2015).
- [26] A. Chiocchetta, M. Tavora, A. Gambassi, and A. Mitra, Short-time universal scaling and light-cone dynamics after a quench in an isolated quantum system in  $d$  spatial dimensions, *Phys. Rev. B* **94**, 134311 (2016).
- [27] P. Calabrese and J. Cardy, Quantum quenches in 1+1 dimensional conformal field theories, *J. Stat. Mech.* (2016) 064003.
- [28] D. Bernard and B. Doyon, Conformal field theory out of equilibrium: a review, *J. Stat. Mech.* (2016) 064005.
- [29] E. Ilievski, M. Medenjak, T. Prosen, and L. Zadnik, Quasilocal charges in integrable lattice systems, *J. Stat. Mech.* (2016) 064008.
- [30] T. Langen, T. Gasenzer, and J. Schmiedmayer, Prethermalization and universal dynamics in near-integrable quantum systems, *J. Stat. Mech.* (2016) 064009.
- [31] R. Vasseur and J. E. Moore, Nonequilibrium quantum dynamics and transport: from integrability to many-body localization, *J. Stat. Mech.* (2016) 064010.
- [32] A. Nahum, J. Ruhman, S. Vijay, and J. Haah, Quantum Entanglement Growth under Random Unitary Dynamics, *Phys. Rev. X* **7**, 031016 (2017).
- [33] M. Heyl, Dynamical quantum phase transitions: a review, *Rep. Prog. Phys.* **81**, 054001 (2018).
- [34] A. Pelissetto, D. Rossini, and E. Vicari, Dynamic finite-size scaling after a quench at quantum transitions, *Phys. Rev. E* **97**, 052148 (2018).
- [35] D. Nigro, D. Rossini, and E. Vicari, Scaling properties of work fluctuations after quenches near quantum transitions, *J. Stat. Mech.* (2019) 023104.
- [36] D. Nigro, D. Rossini, and E. Vicari, Competing coherent and dissipative dynamics close to quantum criticality, *Phys. Rev. A* **100**, 052108 (2019); D. Rossini and E. Vicari, Scaling behavior of stationary states arising from dissipation at continuous quantum transitions, *Phys. Rev. B* **100**, 174303 (2019).
- [37] J. Surace, L. Tagliacozzo, and E. Tonni, Operator content of entanglement spectra in the transverse field Ising chain after global quenches, *Phys. Rev. B* **101**, 241107(R) (2020).
- [38] D. Rossini and E. Vicari, Measurement-induced dynamics of many-body systems at quantum criticality, *Phys. Rev. B* **102**, 035119 (2020).
- [39] S. L. Sondhi, S. M. Girvin, J. P. Carini, and D. Shahar, Continuous quantum phase transitions, *Rev. Mod. Phys.* **69**, 315 (1997).
- [40] S. Sachdev, *Quantum Phase Transitions*, (Cambridge University, Cambridge, England, 1999).
- [41] T. W. B. Kibble, Topology of cosmic domains and strings, *J. Phys. A* **9**, 1387 (1976).
- [42] W. H. Zurek, Cosmological Experiments in Superfluid Helium?, *Nature* **317**, 505 (1985).
- [43] W. H. Zurek, U. Dorner, and P. Zoller, Dynamics of a quantum phase transition, *Phys. Rev. Lett.* **95**, 105701 (2005).
- [44] A. Polkovnikov and V. Gritsev, Breakdown of the adiabatic limit in low-dimensional gapless systems, *Nature Phys.* **4**, 477 (2008).
- [45] A. Chandran, A. Erez, S. S. Gubser, and S. L. Sondhi, Kibble-Zurek problem: Universality and the scaling limit, *Phys. Rev. B* **86**, 064304 (2012).
- [46] D. Rossini and E. Vicari, Dynamic Kibble-Zurek scaling framework for open dissipative many-body systems crossing quantum transitions, *Phys. Rev. Research* **2**, 023211 (2020).
- [47] S. Bhattacharyya, S. Dasgupta, and A. Das, Signature of a continuous quantum phase transition in non-equilibrium energy absorption: Footprints of criticality on higher excited states, *Sci. Rep.* **5**, 16490 (2015).
- [48] S. Roy, R. Moessner, and A. Das, Locating topological phase transitions using nonequilibrium signatures in local bulk observables, *Phys. Rev. B* **95**, 041105(R) (2017).
- [49] P. Titum, J. T. Iosue, J. R. Garrison, A. V. Gorshkov, and Z.-X. Gong, Probing Ground-State Phase Transitions through Quench Dynamics, *Phys. Rev. Lett.* **123**, 115701 (2019).
- [50] M. Heyl, F. Pollmann, and B. Dora, Detecting Equilibrium and Dynamical Quantum Phase Transitions in Ising Chains via Out-of-Time-Ordered Correlators, *Phys. Rev. Lett.* **121**, 016801 (2018).
- [51] A. Haldar, K. Mallayya, M. Heyl, F. Pollmann, M. Rigol, and A. Das, Signatures of quantum phase transitions after quenches in quantum chaotic one-dimensional systems, *arXiv:2004.02905*.
- [52] A. Pelissetto, D. Rossini, and E. Vicari, Scaling properties of the dynamics at first-order quantum transitions when boundary conditions favor one of the two phases, *Phys. Rev. E* **102**, 012143 (2020).
- [53] J. Häppölä, G. B. Halász, and A. Hamma, Universality and robustness of revivals in the transverse field XY model, *Phys. Rev. A* **85**, 032114 (2012).
- [54] P. L. Krapivsky, J. M. Luck, and K. Mallick, Survival of Classical and Quantum Particles in the Presence of Traps, *J. Stat. Phys.* **154**, 1430 (2014).
- [55] J. Cardy, Thermalization and Revivals after a Quantum Quench in Conformal Field Theory, *Phys. Rev. Lett.* **112**, 220401 (2014).
- [56] R. Jafari and H. Johannesson, Loschmidt Echo Revivals: Critical and Noncritical, *Phys. Rev. Lett.* **118**, 015701 (2017).
- [57] R. Modak, V. Alba, and P. Calabrese, Entanglement revivals as a probe of scrambling in finite quantum systems,



- J. Stat. Mech. (2020) 083110.
- [58] H.-P. Breuer and F. Petruccione, *The Theory of Open Quantum Systems* (Oxford University Press, New York, 2002).
  - [59] M. Campostrini, A. Pelissetto, and E. Vicari, Finite-size scaling at quantum transitions, Phys. Rev. B **89**, 094516 (2014).
  - [60] A. Yu. Kitaev, Unpaired Majorana fermions in quantum wires, Phys. Usp. **44**, 131 (2001).
  - [61] E. H. Lieb and D. W. Robinson, The finite group velocity of quantum spin systems, Commun. Math. Phys. **28**, 251 (1972).
  - [62] P. Calabrese and J. Cardy, Evolution of Entanglement Entropy in One-Dimensional Systems, J. Stat. Mech. (2005) P04010.
  - [63] G. Lindblad, On the generators of quantum dynamical semigroups, Commun. Math. Phys. **48**, 119 (1976).
  - [64] V. Gorini, A. Kossakowski, and E. C. G. Sudarshan, Completely positive dynamical semigroups of N-level systems, J. Math. Phys. **17**, 821 (1976).
  - [65] B. Horstmann, J. I. Cirac, and G. Giedke, Noise-driven dynamics and phase transitions in fermionic systems, Phys. Rev. A **87**, 012108 (2013).
  - [66] E. B. Davies, Quantum stochastic processes II, Commun. Math. Phys. **19**, 83 (1970); Quantum stochastic processes, Commun. Math. Phys. **15**, 277 (1969).
  - [67] D. E. Evans, Irreducible Quantum Dynamical Semigroups, Commun. math. Phys. **54**, 293 (1977).
  - [68] S. G. Schirmer and X. Wang, Stabilizing open quantum systems by Markovian reservoir engineering, Phys. Rev. A **81**, 062306 (2010).
  - [69] D. Nigro, On the uniqueness of the steady-state solution of the Lindblad-Gorini-Kossakowski-Sudarshan equation, J. Stat. Mech. (2019) 043202.
  - [70] N. Wu, Longitudinal magnetization dynamics in the quantum Ising ring: A Pfaffian method based on correspondence between momentum space and real space, Phys. Rev. E **101**, 042108 (2020).
  - [71] M. Beccaria, M. Campostrini, and A. Feo, Density-matrix renormalization-group study of the disorder line in the quantum axial next-nearest-neighbor Ising model, Phys. Rev. B **73**, 052402 (2006).
  - [72] P. R. Colares Guimarães, J. A. Plascak, F. C. Sá Barreto, and J. Florencio, Quantum phase transitions in the one-dimensional transverse Ising model with second-neighbor interactions, Phys. Rev. B **66**, 064413 (2002).